Dynamics and Adaptive Control for Stability Recovery of Damaged Asymmetric Aircraft

Nhan Nguyen[*]
Kalmanje Krishnakumar[†]
John Kaneshige[‡]
NASA Ames Research Center, Moffett Field, CA 94035
Pascal Nespeca[§]
University of California, Davis, CA 95616

This paper presents a recent study of a damaged generic transport model as part of a NASA research project to investigate adaptive control methods for stability recovery of damaged aircraft operating in off-nominal flight conditions under damage and or failures. Aerodynamic modeling of damage effects is performed using an aerodynamic code to assess changes in the stability and control derivatives of a generic transport aircraft. Certain types of damage such as damage to one of the wings or horizontal stabilizers can cause the aircraft to become asymmetric, thus resulting in a coupling between the longitudinal and lateral motions. Flight dynamics for a general asymmetric aircraft is derived to account for changes in the center of gravity that can compromise the stability of the damaged aircraft. An iterative trim analysis for the translational motion is developed to refine the trim procedure by accounting for the effects of the control surface deflection. A hybrid direct-indirect neural network, adaptive flight control is proposed as an adaptive law for stabilizing the rotational motion of the damaged aircraft. The indirect adaptation is designed to estimate the plant dynamics of the damaged aircraft in conjunction with the direct adaptation that computes the control augmentation. Two approaches are presented: 1) an adaptive law derived from the Lyapunov stability theory to ensure that the signals are bounded, and 2) a recursive least-square method for parameter identification. A hardware-in-the-loop simulation is conducted and demonstrates the effectiveness of the direct neural network adaptive flight control in the stability recovery of the damaged aircraft. A preliminary simulation of the hybrid adaptive flight control has been performed and initial data have shown the effectiveness of the proposed hybrid approach. Future work will include further investigations and high-fidelity simulations of the proposed hybrid adaptive flight control approach.

I.   Introduction

Aviation safety research concerns with many aspects of safe, reliable flight performance and operation of today's modern aircraft to maintain safe air transportation for the traveling public. While air travel remains the safest mode of transportation, accidents do occur in rare occasions that serve to remind that much work is still remained to be done in aviation safety research. American Airlines Flight 587 illustrates the reality of hazards due to structural failures of airframe components that can cause a catastrophic loss of control.[1] Not all structural damages result in a loss of control. The World War II aviation history filled with many stories of aircraft coming back home safely despite suffering major structural damage to their airframes. Recently, the DHL incident involving an Airbus A300-B4 cargo aircraft in 2003 further illustrates the ability to maintain a controlled flight in the presence of structural damage and hydraulic loss.[2]

In damage events, significant portions of the aircraft's aerodynamic lifting surfaces may become separated and as a result this may cause the aircraft's carefully designed center of gravity (C.G.) to shift unexpectedly. The combined

---

[*]Computer Scientist, Intelligent Systems Division, Mail Stop 269-1
[†]Computer Scientist, Intelligent Systems Division, Mail Stop 269-1
[‡]Computer Engineer, Intelligent Systems Division, Mail Stop 269-1
[§]Ph.D. Student, Mechanical Engineering Department

American Institute of Aeronautics and Astronautics

loss of lift, mass change, and C.G. shift can manifest in an unstable, off-nominal flight condition resulting from the aircraft being out of trim that can adversely affect the ability for an existing flight control system to maintain the aircraft stability. In some other instances, aircraft's damaged structures may suffer losses in structural rigidity and may develop elastic motions that can potentially interfere with an existing flight control system in an unpredictable manner. Moreover, the load carrying capacity of damaged structures may also become impaired and therefore can potentially result in excessive structural loading on critical lifting surfaces due to flight control inputs by the unaware pilot. Thus, in a highly dynamic and difficult off-nominal flight environment with many uncertainties caused by damages to the aircraft, the inner-loop flight control must be able to cope with complex and uncertain aircraft responses that can greatly challenge an existing flight control system.

Flight control of damaged aircraft in off-nominal flight conditions poses significant technical challenges in many areas of disciplines including aerodynamics, structural dynamics, flight dynamics and control, as well as human factors. Thus, a comprehensive investigation from the aircraft integrated system perspective is needed to research and develop adaptive flight control technologies that can be used to retrofit conventional flight control systems in order to enable aircraft to achieve safe flight objectives. This comprehensive investigation would provide an integrated approach to damage effect physics-based modeling and simulation, safety-of-flight assessment, flight control and recovery, and adaptive system verification and validation. Damage effect physics-based modeling generates a knowledge base for understanding the behavior of damaged aircraft performance in the areas of flight mechanics, aerodynamics, and structural dynamics to address system interactions among various sub-systems such as aircraft dynamics, airframe structures, engines, and flight control actuators. Using this knowledge base, flight mechanics of the damaged vehicle can be evaluated by flight simulation to assess classes of damage that can be recovered with different types of flight control effectors. On-board modeling provides state assessments of damaged aircraft in-flight that can be used to aide pilot's decisions and control. Adaptive flight control is a critical technology that enables damaged aircraft to recover post-damage flight stability. Research in neural network adaptive flight control provides a possibility for developing an effective damage adaptive control strategy that can adapt the damaged aircraft to changes in the vehicle stability and control characteristics.[3] Emergency flight planning and post-damage landing technologies are also investigated to aide pilots with an intelligent decision support system to identify a suitable landing site, flight path planning under a reduced flight envelope, and ultimately a safe landing execution strategy.[4] While adaptive flight control has been much researched, it has not been universally adopted in the aviation industry due to a number of software and stability issues that are inherent with any adaptive flight control system. Certification of these adaptive flight control systems is a major hurdle that needs to be overcome. Thus, research in adaptive system verification and validation is needed in order to develop stability and certification requirements for new adaptive flight control methods.[5]

This paper focuses on the flight mechanics and the adaptive flight control of damaged aircraft. The damage nature is primarily due to changes in the aerodynamic configuration of the vehicle brought about by various modes of damage that include airframe and flight control surfaces. Some of these types of damage can cause a rapid loss of vehicle stability and control resulting from a significant loss of lift capability and/or a loss of control power. A flight dynamics model for a damaged aircraft is developed to account for various damage effects including changes in aerodynamics, mass, inertias, and C.G. A trim analysis is presented to enable a rapid estimation of new trim states to maintain the aircraft flight conditions. Damage adaptive flight control methods are developed to enable stability recovery of the damaged aircraft. Research in the adaptive reconfigurable flight control provides a method of risk mitigation for certain types of damage. Recent advances in neural network, direct adaptive flight control provide a foundation for much of this research.[7, 11, 12] A hybrid direct-indirect adaptive control method is proposed to extend the current capability of the neural network adaptive flight control. The hybrid adaptive control includes an indirect adaptive law that performs an on-line estimation of plant dynamics of the damaged aircraft. The stability of this indirect adaptive law is established by the Lyapunov stability theory. An alternative approach is also presented whereby a recursive least-square method is used for the parameter identification process.

II.   Damage Effect Modeling

A twin-engine transport-class generic aircraft is chosen as a platform for the damage effect modeling. We will refer to this notational aircraft as a Generic Transport Model (GTM). Fig. 1 is an illustration of the GTM. Damage to an aircraft airframe and/or control surfaces can cause the aircraft to be out of trim, which consequently can lead to dynamic upsets of the aircraft flight states. Understanding the aircraft aerodynamic characteristics during a damage event is critical to developing flight control strategies for the stability recovery of a damaged aircraft. In order to assess the damage effects on the GTM, aerodynamic modeling is performed to estimate the aerodynamic coefficients, and the

American Institute of Aeronautics and Astronautics

stability and control derivatives of the damaged GTM for various damage configurations under consideration. Damage aerodynamic characteristics will then be incorporated into a flight dynamic model of the damaged aircraft that will be used to develop adaptive flight control strategies. A controllability study can be performed using the flight dynamic model to determine which damage configurations are controllable and those that cannot be controlled.

The damage effect aerodynamic modeling is performed using a vortex-lattice code developed at NASA Ames Research Center.[6] This computational fluid dynamics modeling is capable of rapidly computing the aerodynamic characteristics and control sensitivity of the damaged GTM due to various flight control surface inputs. The damage effects are modeled as partial losses of the left wing, left horizontal stabilizer, and vertical stabilizer, as shown in Fig. 1. Wing loss represents one of the critical modes of damage that is a current focus of the research.
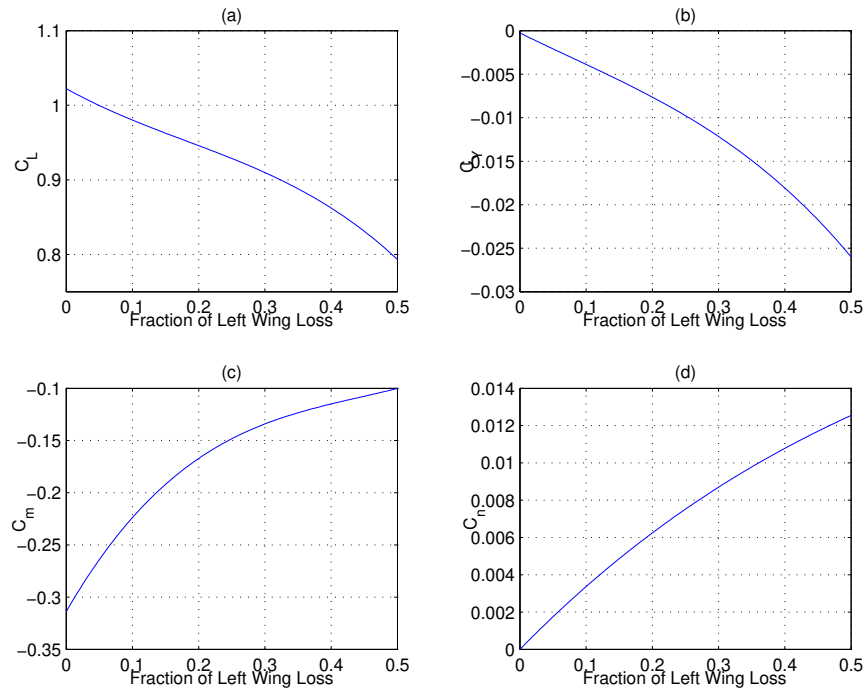

Fig. 1 - Generic Transport Model

Fig. 2 - Aerodynamic Coefficients Due to Wing Loss at $\alpha = 12^{\circ}$ and $\beta = 0^{\circ}$

Fig. 2 shows the damage effect due to wing loss for the damaged GTM. The effect of wing loss can be seen as a significant source of loss of lift capability of a damaged aircraft as the lift coefficient can be reduced by as much as 25% for up to a 50% span loss of one of the wings. Changes in the pitching moment coefficient are also a result of the wing loss. Changing lift and pitch moment causes the aircraft to be out of trim that leads to the inability for the

American Institute of Aeronautics and Astronautics

flight control system to hold altitude and flight path angle. Moreover, the aircraft lateral motion becomes a factor as a significant side force and yawing moment develop without any aileron or rudder input. This lateral motion causes the longitudinal and lateral motions of the damaged aircraft to couple, resulting in changes in the angular rates. The stability of the damaged aircraft can be regained if sufficient control powers are still available to overcome the rolling and yawing moments as well as to retrim the aircraft in the pitch axis.
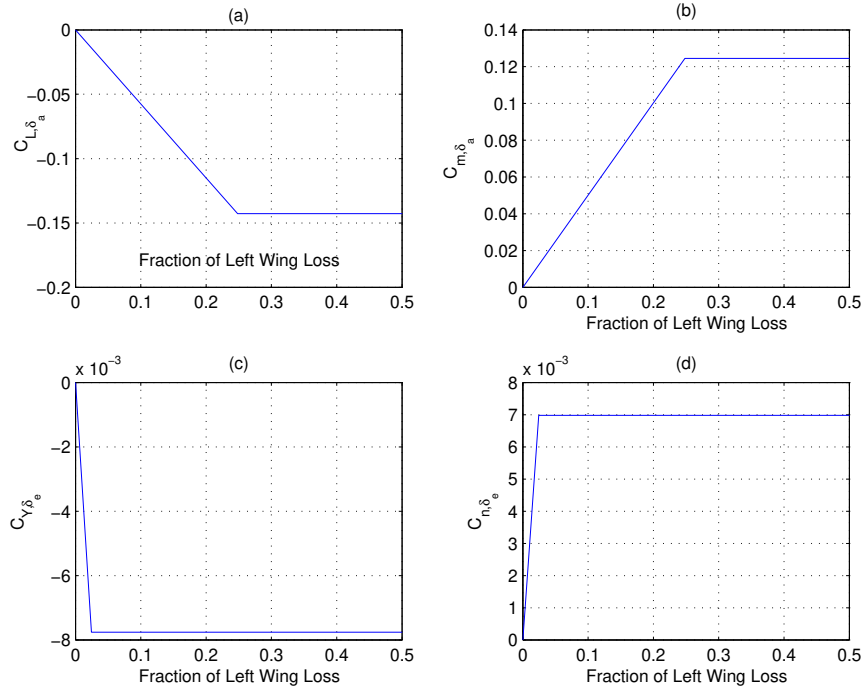

Fig. 3 - Control Derivatives Due to Wing Loss at $\alpha = 12^{\circ}$ and $\beta = 0^{\circ}$

For an ideal symmetric aircraft, the aileron deflection effects the roll control with insignificant contribution to the lift and pitching moment coefficients. The effect of wing loss causes the aileron deflection to induce a change in the lift coefficient as well as a change in the pitching moment coefficients as seen in Fig. 3(a)-(b). The abrupt changes in the lift control and pitch control derivatives are due to the complete loss of one of the ailerons for a wing loss that extends beyond 25% span. The consequence of this is that the damaged aircraft would exhibit a pitch-roll coupling when the ailerons are deflected asymmetrically. To maintain a trim state, the flight control must compensate for the unwanted pitch motion with the elevators. The situation is similar for the elevator control as the effect of wing loss introduces a change in the side force coefficient and a change in the yawing moment coefficient as seen in Fig. 3(c)-(d). Thus, a deflection of the elevators would result in a pitch-yaw coupling that must be compensated within the flight control system by adjusting the rudder control accordingly. Because of the asymmetry, the general motion of a damaged aircraft is coupled in all the three axes. As a result, any adaptive flight control strategy must be able to effectively handle this cross-coupled effect.

III.   Flight Dynamics of Asymmetric Aircraft

The longitudinal motion of a symmetric aircraft is typically symmetric with respect to the aircraft fuselage reference line. The lateral motion is uncoupled from the longitudinal motion owing to the aircraft symmetry. For a damaged aircraft, the symmetry may no longer be preserved depending on the nature of the damage such as wing damage. The asymmetry of the damaged aircraft thus causes the longitudinal motion and lateral motion to couple together. Furthermore, the C.G. is shifted away from the $x - z$ plane. The motion of an asymmetric damaged aircraft, therefore, must be understood in order to evaluate any flight control design. To this end, we consider an asymmetric aircraft with a C.G. offset from some reference location as shown in Fig. 4. The reference location is a fixed point located at the coordinate (x_0, y_0, z_0) on the aircraft which may be taken as the original C.G. of the undamaged aircraft

American Institute of Aeronautics and Astronautics

in order to maintain the same coordinate reference frame. The C.G. of the damaged aircraft can move relative to this fixed reference point.
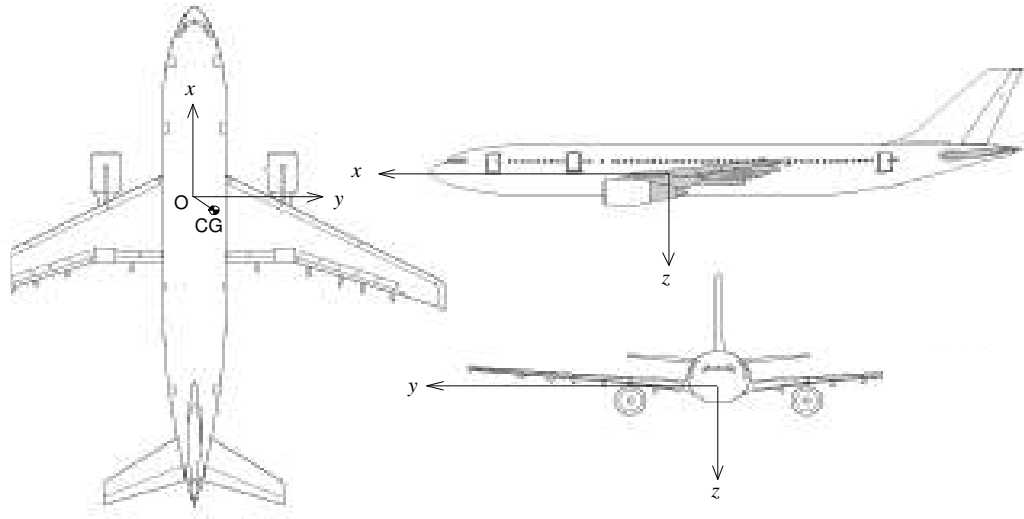
Fig. 4 - C.G. Shift Relative to Reference Point O

The damage effect resulting from a wing loss creates a larger C.G. shift in the pitch axis y than in the other two axes as shown in Fig. 5. This results in an additional rolling moment that the flight control must be able to compensate for using the available control surfaces in order to maintain the damaged aircraft in a trim state.
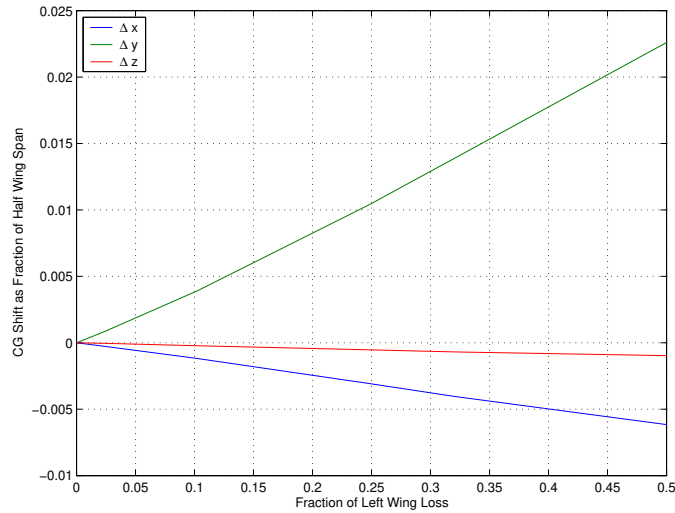
Fig. 5 - C.G. Shift due to Wing Loss

A. Linear Acceleration

To understand the effect of the C.G. shift, the standard equations of motion for flight dynamics of a symmetric aircraft must be modified to allow for the asymmetry. Assuming a flat-earth model for a rigid body aircraft, the force vector in the body-fixed reference frame of the aircraft is

$$\mathbf{F}_B = m\frac{d\mathbf{v}}{dt} + \frac{d}{dt}\left(\boldsymbol{\omega} \times \int \mathbf{r}dm\right) - \mathbf{W} \tag{1}$$

American Institute of Aeronautics and Astronautics

where $\mathbf{W} = mg \begin{bmatrix} -\sin\theta & \cos\theta\sin\phi & \cos\theta\cos\phi \end{bmatrix}^T$ is the gravitational force vector, $\boldsymbol{\omega} = \begin{bmatrix} p & q & r \end{bmatrix}^T$ is the aircraft angular rate vector, $\mathbf{r} = \bar{\mathbf{r}} + \Delta\mathbf{r}$ is the position vector of the reference location such that $\bar{\mathbf{r}}$ is the position vector of the C.G. and $\Delta\mathbf{r} = \begin{bmatrix} \Delta x & \Delta y & \Delta z \end{bmatrix}^T$ is the displacement vector from the C.G. to the reference location.

The aircraft mass is assumed to undergo a change so that

$$m = m^* + \Delta m \tag{2}$$

where m^* is the original mass of the aircraft and $\Delta m < 0$ is the mass change due to damages.

Assuming that the change in the mass of the aircraft is instantaneous, the force vector then becomes

$$\mathbf{F}_B = m\frac{d\mathbf{v}}{dt} + m\frac{d\boldsymbol{\omega}}{dt} \times \Delta\mathbf{r} + m\boldsymbol{\omega} \times \frac{d\Delta\mathbf{r}}{dt} - \mathbf{W} \tag{3}$$

where $\frac{d\Delta\mathbf{r}}{dt}$ is the speed of the C.G. relative to the reference location which is assumed to be small relative to $\mathbf{v}$ and therefore may be neglected.

Transforming from the body-fixed reference frame to the inertial reference frame yields

$$\mathbf{F} = \mathbf{F}_B + m\boldsymbol{\omega} \times \mathbf{v} \tag{4}$$

Expanding Eq. (4) gives

$$X = m\left(\dot{u} + \dot{q}\Delta z - \dot{r}\Delta y - rv + qw + g\sin\theta\right) \tag{5}$$
$$Y = m\left(\dot{v} - \dot{p}\Delta z + \dot{r}\Delta x + ru - pw - g\cos\theta\sin\phi\right) \tag{6}$$
$$Z = m\left(\dot{w} + \dot{p}\Delta y - \dot{q}\Delta x - qu + pv - g\cos\theta\cos\phi\right) \tag{7}$$

The angular acceleration terms appearing in Eqs. (5)-(7) are a result of the C.G. shift. Thus, the linear acceleration of an asymmetric aircraft is coupled with its angular acceleration.

B. Angular Acceleration

We consider the angular momentum vector in the body-fixed reference frame

$$\mathbf{H}_B = \int \left[\mathbf{r} \times (\boldsymbol{\omega} \times \mathbf{r})\right] dm + \int (\mathbf{r} \times \mathbf{v})\, dm \tag{8}$$

Expanding this expression yields

$$\mathbf{H}_B = \mathbf{I}\boldsymbol{\omega} + m\Delta\mathbf{r} \times \mathbf{v} \tag{9}$$

where $\mathbf{I}$ is the mass moment of inertia matrix with respect to the reference frame at the reference location.

The time rate of change in the angular momentum gives rise to the moment equation in the inertial reference frame

$$\mathbf{M} = \frac{d\mathbf{H}_B}{dt} + \boldsymbol{\omega} \times \mathbf{H}_B = \mathbf{I}\frac{d\boldsymbol{\omega}}{dt} + m\Delta\mathbf{r} \times \frac{d\mathbf{v}}{dt} + \boldsymbol{\omega} \times \mathbf{I}\boldsymbol{\omega} + m\boldsymbol{\omega} \times (\Delta\mathbf{r} \times \mathbf{v}) \tag{10}$$

Expanding Eq. (10) results in the following moment equations

$$L = I_{xx}\dot{p} - I_{xy}\dot{q} - I_{xz}\dot{r} + I_{xy}pr - I_{xz}pq + (I_{zz} - I_{yy})\, qr + I_{yz}\left(r^2 - q^2\right)$$
$$\qquad\qquad + m\left(qv + rw\right)\Delta x + m\left(\dot{w} - qu\right)\Delta y - m\left(\dot{v} + ru\right)\Delta z \tag{11}$$

$$M = -I_{xy}\dot{p} + I_{yy}\dot{q} - I_{yz}\dot{r} + I_{yz}pq - I_{xy}qr + (I_{xx} - I_{zz})\, pr + I_{xz}\left(p^2 - r^2\right)$$
$$\qquad\qquad - m\left(\dot{w} + pv\right)\Delta x + m\left(pu + rw\right)\Delta y + m\left(\dot{u} - rv\right)\Delta z \tag{12}$$

$$N = -I_{xz}\dot{p} - I_{yz}\dot{q} + I_{zz}\dot{r} + I_{xz}qr - I_{yz}pr + (I_{yy} - I_{xx})\, pq + I_{xy}\left(q^2 - p^2\right)$$
$$\qquad\qquad + m\left(\dot{v} - pw\right)\Delta x - m\left(\dot{u} + qw\right)\Delta y + m\left(pu + qv\right)\Delta z \tag{13}$$

Equations (11)-(13) indicate that the C.G. offset effectively creates additional moments on the aircraft. Cross coupling in both the linear and angular accelerations are present. Thus, the longitudinal and lateral motions of the aircraft are generally coupled and the aileron or elevator commanded input therefore will affect the aircraft motion in both stability axes.

American Institute of Aeronautics and Astronautics

C. Aerodynamic and Propulsive Forces and Moments

Assuming that the engine thrust vector is aligned with the x-axis of the aircraft, then the forces and moments due to aerodynamics and the propulsion are

$$X = \delta_T T_{max} + (C_L^* + \Delta C_L)\, QS \sin\alpha - (C_D^* + \Delta C_D)\, QS \cos\alpha \cos\beta \tag{14}$$

$$Y = (C_Y^* + \Delta C_Y)\, QS - (C_D^* + \Delta C_D)\, QS \sin\beta \tag{15}$$

$$Z = -(C_L^* + \Delta C_L)\, QS \cos\alpha - (C_D^* + \Delta C_D)\, QS \sin\alpha \cos\beta \tag{16}$$

$$L = (C_l^* + \Delta C_l)\, QS\bar{c} \tag{17}$$

$$M = (C_m^* + \Delta C_m)\, QS\bar{c} + \delta_T T_{max} (z_e - z_0) \tag{18}$$

$$N = (C_n^* + \Delta C_n)\, QS\bar{c} + \delta_{\Delta T} T_{max} y_e + \delta_T T_{max} y_0 \tag{19}$$

where $(x_e, \pm y_e, z_e)$ are the centers of thrust and the subscript * denotes the force and moment coefficients for the undamaged aircraft evaluated at the reference location.

We assume that the left and right engines produce the same amount of thrust with a combined maximum thrust equal to T_{max} and are symmetrically positioned with respect to the aircraft fuselage reference line. Then δ_T where $0 \leq \delta_T \leq 1$ is the throttle position corresponding to a desired total engine thrust, and $\delta_{\Delta T}$ where $-\frac{1}{2} \leq \delta_{\Delta T} \leq \frac{1}{2}$ is the throttle differential position difference that results in a desired engine differential thrust equal to the left engine thrust minus the right engine thrust. The incremental changes in these coefficients due to damages are defined as

$$\Delta\mathbf{C} = \Delta\mathbf{C}_0 + \Delta\mathbf{C}_\alpha \alpha + \Delta\mathbf{C}_\beta \beta + \Delta\mathbf{C}_{\boldsymbol\delta} \boldsymbol\delta \tag{20}$$

where $\Delta\mathbf{C} = \begin{bmatrix} C_L - C_L^* & C_D - C_D^* & C_Y - C_Y^* & C_l - C_l^* & C_m - C_m^* & C_n - C_n^* \end{bmatrix}^T$, $\boldsymbol\delta = \begin{bmatrix} \delta_a & \delta_e & \delta_r \end{bmatrix}^T$ is the flight control surface deflection vector, the subscripts α, β, and $\boldsymbol\delta$ denote the derivatives, and the subscript 0 denotes the coefficients at $\alpha = 0$ and $\beta = 0$.

IV. Trim Analysis

The aerodynamic forces on asymmetric aircraft include a non-zero side force component that is generally not experienced on symmetric aircraft. For a steady flight, the side force equation becomes

$$mg\cos\theta\sin\phi + (C_Y^* + \Delta C_Y)\, QS - (C_D^* + \Delta C_D)\, QS \sin\beta = 0 \tag{21}$$

The side force trim for the asymmetric aircraft can therefore be accomplished by trimming the aircraft at a non-zero bank angle ϕ with zero sideslip angle β. However, this would result in a limitation in the bank angle in coordinated turn maneuvers. Another side force trim approach is to trim the aircraft level with zero bank angle ϕ but at a non-zero sideslip angle β. In either case, the aircraft would have to be trimmed in both the longitudinal and lateral directions simultaneously by searching for the steady state solution of Eqs. (14) to (16) with $\phi = 0$ or $\beta = 0$. The trim analysis thus computes the trim values for the angle of attack α, bank angle ϕ or sideslip angle β, and engine throttle position δ_T as functions of the aileron deflection δ_a, elevator deflection δ_e, and rudder deflection δ_r for a given aircraft Mach number and altitude. We assume that the engine thrusts will be symmetric at all times so that $\delta_{\Delta T} = 0$.

If an undamaged symmetric aircraft has a mass m^* and is flying wing-level, i.e., $\phi^* = 0$, with zero control surface deflection at the original trim angle of attack α^*, sideslip angle $\beta^* = 0$, and trim throttle position δ_T^* corresponding to a lift coefficient C_L^*, drag coefficient C_D^*, and side force coefficient $C_Y^* = 0$. Then for small changes in the aircraft mass and aerodynamic coefficients, we can determine the incremental trim angle of attack, bank angle, and throttle position to maintain approximately the same trim airspeed V and flight path angle γ^* by taking small but finite differences of Eqs. (14) to (16) and setting them to zero, thus resulting in

$$\Delta\delta_T T_{max} + (\Delta C_L + C_{L,\alpha}\Delta\alpha + C_{L,\beta}\Delta\beta + C_{L,\boldsymbol\delta}\boldsymbol\delta)\, QS \sin\alpha^* + (C_L + C_{L,\alpha}\Delta\alpha + C_{L,\beta}\Delta\beta + C_{L,\boldsymbol\delta}\boldsymbol\delta)\, QS \cos\alpha^* \Delta\alpha$$
$$- (\Delta C_D + C_{D,\alpha}\Delta\alpha + C_{D,\beta}\Delta\beta + C_{D,\boldsymbol\delta}\boldsymbol\delta)\, QS \cos\alpha^* + (C_D + C_{D,\alpha}\Delta\alpha + C_{D,\beta}\Delta\beta + C_{D,\boldsymbol\delta}\boldsymbol\delta)\, QS \sin\alpha^* \Delta\alpha$$
$$- mg \cos(\gamma^* + \alpha^*)\Delta\alpha - \Delta mg \sin(\gamma^* + \alpha^*) = 0 \tag{22}$$

$$(\Delta C_Y + C_{Y,\alpha}\Delta\alpha + C_{Y,\beta}\Delta\beta + C_{Y,\boldsymbol{\delta}}\boldsymbol{\delta})\,QS - (C_D + C_{D,\alpha}\Delta\alpha + C_{D,\beta}\Delta\beta + C_{Y,\boldsymbol{\delta}}\boldsymbol{\delta})\,QS\Delta\beta$$
$$+ mg\left[\cos\left(\gamma^* + \alpha^*\right) - \sin\left(\gamma^* + \alpha^*\right)\Delta\alpha\right]\Delta\phi = 0 \quad (23)$$

$$-(\Delta C_L + C_{L,\alpha}\Delta\alpha + C_{L,\beta}\Delta\beta + C_{L,\boldsymbol{\delta}}\boldsymbol{\delta})\,QS\cos\alpha^* + (C_L + C_{L,\alpha}\Delta\alpha + C_{L,\beta}\Delta\beta + C_{L,\boldsymbol{\delta}}\boldsymbol{\delta})\,QS\sin\alpha^*\Delta\alpha$$
$$-(\Delta C_D + C_{D,\alpha}\Delta\alpha + C_{D,\beta}\Delta\beta + C_{D,\boldsymbol{\delta}}\boldsymbol{\delta})\,QS\sin\alpha^* - (C_D + C_{D,\alpha}\Delta\alpha + C_{D,\beta}\Delta\beta + C_{D,\boldsymbol{\delta}}\boldsymbol{\delta})\,QS\cos\alpha^*\Delta\alpha$$
$$- mg\sin\left(\gamma^* + \alpha^*\right)\Delta\alpha + \Delta mg\cos\left(\gamma^* + \alpha^*\right) = 0 \quad (24)$$

To find the trim bank angle at zero sideslip angle, we set $\Delta\beta = 0$ in the equations above. Equation (24) then is a quadratic equation in terms of $\Delta\alpha$ whose solution can easily be computed as

$$\Delta\alpha = -\frac{b}{2a} + \sqrt{\left(\frac{b}{2a}\right)^2 - \frac{c}{a}} \quad (25)$$

with

$$a = (C_{L,\alpha}\sin\alpha^* - C_{D,\alpha}\cos\alpha^*)\,QS \quad (26)$$
$$b = [(C_L + C_{L,\boldsymbol{\delta}}\boldsymbol{\delta} - C_{D,\alpha})\sin\alpha^* - (C_D + C_{D,\boldsymbol{\delta}}\boldsymbol{\delta} + C_{L,\alpha})\cos\alpha^*]\,QS - mg\sin\left(\gamma^* + \alpha^*\right) \quad (27)$$
$$c = -[(\Delta C_L + C_{L,\boldsymbol{\delta}}\boldsymbol{\delta})\cos\alpha^* + (\Delta C_D + C_{D,\boldsymbol{\delta}}\boldsymbol{\delta})\sin\alpha^*]\,QS + \Delta mg\cos\left(\gamma^* + \alpha^*\right) \quad (28)$$

From Eq. (23), we now find the trim bank angle

$$\Delta\phi = \frac{-\left(\Delta C_Y + C_{Y,\alpha}\Delta\alpha + C_{Y,\boldsymbol{\delta}}\boldsymbol{\delta}\right)QS}{mg\left[\cos\left(\gamma^* + \alpha^*\right) - \sin\left(\gamma^* + \alpha^*\right)\Delta\alpha\right]} \quad (29)$$

Finally, the incremental trim throttle position can be solved directly from Eq. (22).

Trimming the damaged aircraft with bank angle will result in a reduced bank angle limitation. This would potentially affect the aircraft's turn capability. Moreover, the aircraft will not fly wing-level which would not be acceptable for a landing approach. Therefore, the damaged aircraft can be trimmed alternatively with the sideslip angle. This will enable the aircraft to maintain a level flight but the control authority of the rudder control surface will be reduced since it has to compensate for the non-zero sideslip angle. To obtain the trim sideslip angle, we set $\Delta\phi = 0$ in the Eq. (23) and solve Eqs. (22) to (24) simultaneously.

In examining Eq. (23) with $\Delta\phi = 0$, it is noted that if the undamaged aircraft is in a cruise phase at a minimum drag, then the trim sideslip angle for the damaged aircraft could be large if the damage develops a significant side force. Typically, it is not advisable to fly the aircraft at a high sideslip angle because of the stability issue. Depending on the extent of damages, an effective trim approach may be one that uses a combination of the trim bank angle and sideslip angle.

In cases where the rudder control power is insufficient due to damages, then the engine differential thrust throttle position $\delta_{\Delta T}$ could be used to provide an additional control effector to trim the aircraft in yaw. Using engine differential thrust for yaw control requires examining the issue associated with a slow engine response relative to the responses of typical flight control surfaces. While in theory the engine thrust can be used to trim the aircraft in yaw, often by the time the engine thrust is adjusted differentially to the correct trim value, the aircraft may have reached a different dynamic state due to the loss in airspeed and or altitude if the damage condition is severe enough to cause the aircraft performance to rapidly deteriorate in its flight envelope. Because of the time scale difference between traditional flight control surfaces and engines, engine actuator dynamics must be accounted for in the overall flight control strategy.

In addition to using the engine differential thrust as a control effector, other flight control surfaces can be used in an overall control redundancy design strategy. This investigation would examine the control effectiveness of a various combinations of flight control surfaces. For example, wing spoilers can be used for roll control and the wing flap extension or deflection can be used for pitch control. Some of these control surfaces may have different time latency characteristics such as wing flaps versus spoilers. In the control and stability analysis, actuator dynamic model of slow systems should be included in the overall flight dynamic modeling.

The trim analysis shows that upon damage, the damaged aircraft would have to be retrimmed with a new trim angle of attack $\alpha = \alpha^* + \Delta\alpha$, new bank angle $\phi = \Delta\phi$ or new sideslip angle $\beta = \Delta\beta$, and new throttle position $\delta_T = \delta_T^* + \Delta\delta_T$. The trim α, ϕ or β, and δ_T are all functions of the flight control surface deflection $\boldsymbol{\delta}$ as well as the aircraft damage configuration. In general, the stability and control derivatives needed to retrim the damaged aircraft

American Institute of Aeronautics and Astronautics

are not known. Thus, it is necessary that these parameters be identified in flight by a parameter identification process. Assuming that the effect of damage on the aerodynamics can be estimated, then a trim strategy is to initially retrim the damaged aircraft with zero control surface deflection by setting $\delta = 0$ in Eqs. (22) to (24). Then, using the inner-loop rate-command-attitude-hold (RCAH) control, the control surface deflection for the damaged aircraft can be obtained. This allows the trim values to be refined. Depending on the nature of damage, the trim refinement may be repeated until the damaged aircraft becomes completely trimmed.

V. Damage Adaptive Flight Control

Most conventional flight control systems utilize extensive gain-scheduling in order to achieve desired handling qualities. While this approach has proved to be very successful, the development process can be expensive and often results in aircraft specific implementations. Over the past several years, various adaptive control techniques have been investigated.[7] Damaged aircraft presents a challenge to the conventional flight control systems because the aircraft dynamics may deviate from its known dynamics substantially due to a significant degradation in the flight performance of the damaged aircraft. This makes it difficult for the conventional flight control systems to cope with changes in the stability and control of the damaged aircraft. Adaptive flight control provides a possibility for maintaining the stability of a damage aircraft by means of being able to quickly adapt to uncertain system dynamics. Research in adaptive control has spanned several decades, but challenges in obtaining robustness in the presence of unmodeled dynamics, parameter uncertainties, or disturbances as well as the issues with certification, verification and validation of adaptive flight control software prevent it from being implemented in flight control systems.[8] Adaptive control laws may be divided into direct and indirect approaches. Indirect adaptive control methods provide the ability to compute control parameters from on-line neural networks that estimate plant parameters.[9] Parameter identification techniques such as recursive least squares and neural networks have been used in indirect adaptive control methods.[10] In recent years, model-reference direct adaptive control using neural networks has been a topic of great research interests.[11–13] Lyapunov stability theory has been used to establish robustness of neural network adaptive control to ensure that adaption laws for neural network weight updates are asymptotically stable.

In the current research, we adopt the work by Rysdyk and Calise[11] to develop a neural network adaptive control with dynamic inversion for damaged aircraft. The adaptive flight control is able to provide consistent handling qualities without requiring extensive gain-scheduling or explicit system identification for a damaged aircraft. This particular architecture uses both pre-trained and on-line learning neural networks, and reference models to specify desired handling qualities. Pre-trained neural networks are used to provide estimates of aerodynamic stability and control characteristics required for model inversion. On-line learning neural networks are used to compensate for errors and adapt to changes in aircraft dynamics. As a result, consistent handling qualities may be achieved across flight conditions and for different damage configurations. An architecture of the neural network adaptive flight control is shown in Fig. 6. Furthermore, we will extend this architecture to include an indirect adaptive control element that provides an on-line estimation of the true plant dynamics. The estimation approach is provided by an adaptive law based on the Lyapunov stability analysis. In addition, we also consider a recursive least square method for the on-line estimation.
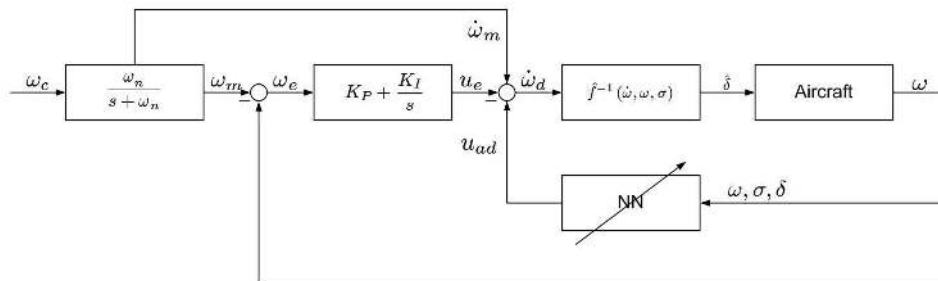

Fig. 6 - Direct Neural Network Adaptive Flight Control Architecture

American Institute of Aeronautics and Astronautics

A. Linearized Plant Dynamics

First, we need to arrive at a linear dynamics of the damaged aircraft for the feedback linearization control. To maintain airspeed and altitude, the damaged aircraft has to be retrimmed using the trim method above. The damaged aircraft stability must be recovered by the RCAH controller. This results in control surface deflections necessary to maintain a desired angular rate command. To design a linear RCAH controller, we want to eliminate the linear acceleration terms in Eqs. (11) to (13) corresponding to the uncompensated damaged aircraft dynamics of linear motion resulting from damages. Combining Eqs. (5) to (7) with Eqs. (11) to (13) yields

$$
\bar{I}_{xx}\dot{p} - \bar{I}_{xy}\dot{q} - \bar{I}_{xz}\dot{r} + I_{xy}pr - I_{xz}pq + (I_{zz} - I_{yy})\,qr + I_{yz}\left(r^2 - q^2\right)
$$
$$
+ m\,(qv + rw)\,\Delta x - mpv\Delta y - mpw\Delta z = \left(C_l^* + \Delta\bar{C}_l\right)QS\bar{c} \quad (30)
$$

$$
-\bar{I}_{xy}\dot{p} + \bar{I}_{yy}\dot{q} - \bar{I}_{yz}\dot{r} + I_{yz}pq - I_{xy}qr + (I_{xx} - I_{zz})\,pr + I_{xz}\left(p^2 - r^2\right)
$$
$$
- mqu\Delta x + m\,(pu + rw)\,\Delta y - mqw\Delta z = \left(C_m^* + \Delta\bar{C}_m\right)QS\bar{c} + \delta_T T_{max}\,(z_e - z_0) \quad (31)
$$

$$
-\bar{I}_{xz}\dot{p} - \bar{I}_{yz}\dot{q} + \bar{I}_{zz}\dot{r} + I_{xz}qr - I_{yz}pr + (I_{yy} - I_{xx})\,pq + I_{xy}\left(q^2 - p^2\right)
$$
$$
- mru\Delta x - mrv\Delta y + m\,(pu + qv)\,\Delta z = \left(C_n^* + \Delta\bar{C}_n\right)QS\bar{c} + \delta_T T_{max}y_0 \quad (32)
$$

where

$$
\Delta\bar{C}_l = \Delta C_l + C_y\frac{\Delta z}{\bar{c}} - C_z\frac{\Delta y}{\bar{c}} - \frac{mg}{QS}\left(\cos\theta\cos\phi\frac{\Delta y}{\bar{c}} - \cos\theta\sin\phi\frac{\Delta z}{\bar{c}}\right) \quad (33)
$$

$$
\Delta\bar{C}_m = \Delta C_m - C_x\frac{\Delta z}{\bar{c}} + C_z\frac{\Delta x}{\bar{c}} + \frac{mg}{QS}\left(\cos\theta\cos\phi\frac{\Delta x}{\bar{c}} + \sin\theta\frac{\Delta z}{\bar{c}}\right) \quad (34)
$$

$$
\Delta\bar{C}_n = \Delta C_n + C_x\frac{\Delta y}{\bar{c}} - C_y\frac{\Delta x}{\bar{c}} - \frac{mg}{QS}\left(\cos\theta\sin\phi\frac{\Delta x}{\bar{c}} + \sin\theta\frac{\Delta y}{\bar{c}}\right) \quad (35)
$$

where C_x, C_y, and C_z are X, Y, and Z force coefficients normalized to the dynamic pressure force QS.

The linear dynamics of the damaged aircraft is computed by linearizing Eqs. (30) to (32)

$$
\left(\bar{\mathbf{I}}^* + \Delta\bar{\mathbf{I}}\right)\frac{d\tilde{\boldsymbol{\omega}}}{dt} = \left(\mathbf{f}_1^* + \Delta\mathbf{f}_1\right)\tilde{\boldsymbol{\omega}} + \left(\mathbf{f}_2^* + \Delta\mathbf{f}_2\right)\boldsymbol{\sigma} + \left(\mathbf{g}^* + \Delta\mathbf{g}\right)\boldsymbol{\delta} \quad (36)
$$

where $\tilde{\boldsymbol{\omega}} = \begin{bmatrix} \Delta p & \Delta q & \Delta r \end{bmatrix}^T$ is the angular rate vector, $\boldsymbol{\sigma} = \begin{bmatrix} \Delta\alpha & \Delta\beta & \Delta\phi & \Delta\delta_T \end{bmatrix}^T$ is the trim parameter vector, and

$$
\mathbf{f}_1^* = QS\bar{c}\begin{bmatrix} C_{l,p}^* & C_{l,q}^* & C_{l,r}^* \\ C_{m,p}^* & C_{m,q}^* & C_{m,r}^* \\ C_{n,p}^* & C_{n,q}^* & C_{n,r}^* \end{bmatrix}
$$

$$
\Delta\mathbf{f}_1 = QS\bar{c}\begin{bmatrix} \Delta\bar{C}_{l,p} & \Delta\bar{C}_{l,q} & \Delta\bar{C}_{l,r} \\ \Delta\bar{C}_{m,p} & \Delta\bar{C}_{m,q} & \Delta\bar{C}_{m,r} \\ \Delta\bar{C}_{n,p} & \Delta\bar{C}_{n,q} & \Delta\bar{C}_{n,r} \end{bmatrix} + m\begin{bmatrix} v\Delta y + w\Delta z & -v\Delta x & -w\Delta x \\ -u\Delta y & u\Delta x + w\Delta z & -w\Delta y \\ -u\Delta z & -v\Delta z & u\Delta x + v\Delta y \end{bmatrix}
$$

$$
\mathbf{f}_2^* = QS\bar{c}\begin{bmatrix} C_{l,\alpha}^* & C_{l,\beta}^* & 0 & 0 \\ C_{m,\alpha}^* + \frac{\delta_T T_{max,\alpha}}{QS}\frac{z_e - z_0}{\bar{c}} & C_{m,\beta}^* + \frac{\delta_T T_{max,\beta}}{QS}\frac{z_e - z_0}{\bar{c}} & 0 & \frac{T_{max}}{QS}\frac{z_e - z_0}{\bar{c}} \\ C_{n,\alpha}^* + \frac{\delta_T T_{max,\alpha}}{QS}\frac{y_0}{\bar{c}} & C_{n,\beta}^* + \frac{\delta_T T_{max,\beta}}{QS}\frac{y_0}{\bar{c}} & 0 & \frac{T_{max}}{QS}\frac{y_0}{\bar{c}} \end{bmatrix}
$$

$$
\Delta\mathbf{f}_2 = QS\bar{c}\begin{bmatrix} \Delta\bar{C}_{l,\alpha} & \Delta\bar{C}_{l,\beta} & \Delta\bar{C}_{l,\phi} & \Delta\bar{C}_{l,\delta_T} \\ \Delta\bar{C}_{m,\alpha} & \Delta\bar{C}_{m,\beta} & \Delta\bar{C}_{l,\phi} & \Delta\bar{C}_{l,\delta_T} \\ \Delta\bar{C}_{n,\alpha} & \Delta\bar{C}_{m,\beta} & \Delta\bar{C}_{l,\phi} & \Delta\bar{C}_{l,\delta_T} \end{bmatrix}
$$

$$\mathbf{g}^* = QS\bar{c} \begin{bmatrix} C^*_{l,\delta_a} & C^*_{l,\delta_e} & C^*_{l,\delta_r} \\ C^*_{m,\delta_a} & C^*_{m,\delta_e} & C^*_{m,\delta_r} \\ C^*_{n,\delta_a} & C^*_{n,\delta_e} & C^*_{n,\delta_r} \end{bmatrix}$$

$$\Delta\mathbf{g} = QS\bar{c} \begin{bmatrix} \Delta\bar{C}_{l,\delta_a} & \Delta\bar{C}_{l,\delta_e} & \Delta\bar{C}_{l,\delta_r} \\ \Delta\bar{C}_{m,\delta_a} & \Delta\bar{C}_{m,\delta_e} & \Delta\bar{C}_{m,\delta_r} \\ \Delta\bar{C}_{n,\delta_a} & \Delta\bar{C}_{n,\delta_e} & \Delta\bar{C}_{n,\delta_r} \end{bmatrix}$$

Equation (36) is the angular acceleration equation of the asymmetric aircraft which can be written in a state-space form as

$$\dot{\tilde{\boldsymbol{\omega}}} = (\mathbf{F}_1 + \Delta\mathbf{F}_1)\,\tilde{\boldsymbol{\omega}} + (\mathbf{F}_2 + \Delta\mathbf{F}_2)\,\boldsymbol{\sigma} + (\mathbf{G} + \Delta\mathbf{G})\,\boldsymbol{\delta} \tag{37}$$

where $\mathbf{F}_1 = \bar{\mathbf{I}}^{*-1}\mathbf{f}_1^*$, $\mathbf{F}_2 = \bar{\mathbf{I}}^{*-1}\mathbf{f}_2^*$, $\mathbf{G} = \bar{\mathbf{I}}^{*-1}\mathbf{g}^*$, $\Delta\mathbf{F}_1 = \bar{\mathbf{I}}^{-1}\left(\mathbf{f}_1^* + \Delta\mathbf{f}_1\right) - \mathbf{F}_1$, $\Delta\mathbf{F}_2 = \bar{\mathbf{I}}^{-1}\left(\mathbf{f}_2^* + \Delta\mathbf{f}_2\right) - \mathbf{F}_2$, and $\Delta\mathbf{G} = \bar{\mathbf{I}}^{-1}\left(\mathbf{g}^* + \Delta\mathbf{g}\right) - \mathbf{G}$.

Under ideal situations, the plant dynamics of an undamaged aircraft is assumed to be known. However, for a damaged aircraft, the plant dynamics become uncertain as the stability and control derivative matrices $\Delta\mathbf{F}_1$, $\Delta\mathbf{F}_2$, and $\Delta\mathbf{G}$ are usually unknown. Consequently, the flight control needs to be able to adapt to the uncertain plant dynamics of the damaged aircraft. The angular acceleration vector $\dot{\tilde{\boldsymbol{\omega}}}$ of the damaged aircraft may be written as the sum of an ideal angular acceleration vector $\dot{\boldsymbol{\omega}}_i$ of the undamaged aircraft and a differential angular acceleration vector $\Delta\dot{\boldsymbol{\omega}}$ due to damage as

$$\dot{\tilde{\boldsymbol{\omega}}} = \dot{\boldsymbol{\omega}}_i + \Delta\dot{\boldsymbol{\omega}} \tag{38}$$

The ideal, undamaged aircraft plant dynamics can be written as

$$\dot{\boldsymbol{\omega}}_i = \mathbf{F}_1\tilde{\boldsymbol{\omega}} + \mathbf{F}_2\boldsymbol{\sigma} + \mathbf{G}\boldsymbol{\delta} \tag{39}$$

where the stability and control matrices for the undamaged aircraft $\mathbf{F}_1$, $\mathbf{F}_2$, and $\mathbf{G}$ are assumed to be known.

B.   Direct Neural Network Adaptive Control

The goal of the adaptive flight control is to be able to fly the damaged aircraft whose handling characteristics is specified by a reference model. The control adaptation must be able to accommodate damages using the available flight control surfaces. A reference model is used to filter a rate command vector $\boldsymbol{\omega}_c$ into a reference angular rate vector $\boldsymbol{\omega}_m$ and a reference angular acceleration vector $\dot{\boldsymbol{\omega}}_m$ via a first-order model

$$\dot{\boldsymbol{\omega}}_m + \boldsymbol{\omega}_n\boldsymbol{\omega}_m = \boldsymbol{\omega}_n\boldsymbol{\omega}_c \tag{40}$$

where $\boldsymbol{\omega}_n = \text{diag}\left(\omega_p, \omega_q, \omega_r\right)$ is the frequency matrix.

The reference frequency parameters must be chosen appropriately in order to obtain a good transient response that satisfies position and rate limits on the control surface deflection. For transport aircraft, typical values of the reference model frequencies ω_p, ω_q, and ω_r are 3.5, 2.5, and 2.0, respectively.[3] In cases when the reference model is over- or under-specified, the parameters of the reference model must be adjusted. The tuning of the reference model parameters can be performed using an adaptive-critic approach to ensure that the flight control can track the reference model in order to achieve desired handling qualities.[16]

The reference model angular rate vector $\boldsymbol{\omega}_m$ are compared with the actual angular rate output $\tilde{\boldsymbol{\omega}}$ to form a tracking error signal $\boldsymbol{\omega}_e = \boldsymbol{\omega}_m - \tilde{\boldsymbol{\omega}}$. A pseudo-feed back control vector $\mathbf{u}_e$ is constructed using a proportional-integral (PI) feedback scheme to better handle errors detected from the roll rate, pitch rate, and yaw rate feedback. The error dynamics, defined by proportional and integral gains, must be fast enough to track the reference model, yet slow enough to not interfere with actuator dynamics. The issue with the integrator windup during a control saturation is addressed by a windup protection which limits the integrator at its current value when a control surface is commanded beyond its limit. The pseudo-control vector $\mathbf{u}_e$ is computed as

$$\mathbf{u}_e = \mathbf{K}_P\boldsymbol{\omega}_e + \mathbf{K}_I \int_0^t \boldsymbol{\omega}_e d\tau \tag{41}$$

In order to ensure low-gain error handling performance, the error dynamics is designed with natural frequencies that match the reference model frequencies in the roll, pitch, and yaw axes. A damping ratio is chosen with $\zeta_p = \zeta_q = \zeta_r = 1/\sqrt{2}$. These frequencies and damping ratio are incorporated into the proportional and integral gains as

$$\mathbf{K}_P = \text{diag}\left(2\zeta_p\omega_p, 2\zeta_q\omega_q, 2\zeta_r\omega_r\right) \tag{42}$$

$$\mathbf{K}_I = \text{diag}\left(\omega_p^2, \omega_q^2, \omega_r^2\right) \tag{43}$$

A dynamic inversion is performed to obtain an estimated control surface deflection command $\hat{\boldsymbol{\delta}}$ to achieve a desired angular acceleration vector $\dot{\boldsymbol{\omega}}_d$ using the known plant dynamics of the undamaged aircraft from Eq. (39) as

$$\hat{\boldsymbol{\delta}} = \mathbf{G}^{-1}\left(\dot{\boldsymbol{\omega}}_d - \mathbf{F}_1\tilde{\boldsymbol{\omega}} - \mathbf{F}_2\boldsymbol{\sigma}\right) \tag{44}$$

assuming that $\mathbf{B}$ is invertible.

In order for the dynamic inversion control to track the reference model angular acceleration rate vector $\dot{\boldsymbol{\omega}}_m$, the desired angular acceleration vector $\dot{\boldsymbol{\omega}}_d$ is set to be equal to

$$\dot{\boldsymbol{\omega}}_d = \dot{\boldsymbol{\omega}}_m + \mathbf{u}_e - \mathbf{u}_{ad} \tag{45}$$

where $\mathbf{u}_{ad}$ is an adaptive control augmentation designed to cancel out the dynamic inversion error, so that in an ideal setting, the desired angular acceleration rate $\dot{\boldsymbol{\omega}}_d$ is equal to the reference model angular acceleration rate $\dot{\boldsymbol{\omega}}_m$ as the tracking error goes to zero asymptotically.

Because the true plant dynamics of the damaged aircraft is unknown and is different from the undamaged aircraft plant dynamics as can be seen from Eq. (37), a dynamic inversion will result from the control surface deflection $\hat{\boldsymbol{\delta}}$. This error is equal to

$$\boldsymbol{\varepsilon} = \dot{\boldsymbol{\omega}} - \dot{\boldsymbol{\omega}}_d = \dot{\boldsymbol{\omega}} - \mathbf{F}_1\tilde{\boldsymbol{\omega}} - \mathbf{F}_2\boldsymbol{\sigma} - \mathbf{G}\hat{\boldsymbol{\delta}} \tag{46}$$

Comparing with Eq. (37), we see that the dynamic inversion error can also be expressed in terms of the unknown plant dynamics due to the damage effects

$$\boldsymbol{\varepsilon} = \Delta\dot{\boldsymbol{\omega}} = \Delta\mathbf{F}_1\tilde{\boldsymbol{\omega}} + \Delta\mathbf{F}_2\boldsymbol{\sigma} + \Delta\mathbf{G}\hat{\boldsymbol{\delta}} \tag{47}$$

Substituting Eq. (45) into Eq. (46) results in

$$\boldsymbol{\varepsilon} = -\dot{\boldsymbol{\omega}}_e - \mathbf{u}_e + \mathbf{u}_{ad} \tag{48}$$

Combining Eq. (41) with Eq. (48) yields

$$\dot{\mathbf{e}} = \mathbf{A}\mathbf{e} + \mathbf{B}\left(\mathbf{u}_{ad} - \boldsymbol{\varepsilon}\right) \tag{49}$$

where $\mathbf{e} = \begin{bmatrix} \int_0^t \boldsymbol{\omega}_e d\tau & \boldsymbol{\omega}_e \end{bmatrix}$ and

$$\mathbf{A} = \begin{bmatrix} \mathbf{0} & \mathbf{I} \\ -\mathbf{K}_I & -\mathbf{K}_P \end{bmatrix}, \ \mathbf{B} = \begin{bmatrix} \mathbf{0} \\ \mathbf{I} \end{bmatrix}$$

The adaptive control augmentation vector $\mathbf{u}_{ad}$ is based on a neural network adaptation law by Rysdyk and Calise[11] that guarantees boundedness of the tracking error and of the network weights using a single-hidden-layer sigma-pi neural network

$$\mathbf{u}_{ad} = \mathbf{W}^T\boldsymbol{\beta}\left(\mathbf{C}_1, \mathbf{C}_2, \mathbf{C}_3\right) \tag{50}$$

where $\boldsymbol{\beta}$ is a vector of basis functions computed using a nested Kronecker product with $\mathbf{C}_1, \mathbf{C}_2, \mathbf{C}_3$ as inputs into the neural network consisting of control commands, sensor feedback, and bias terms.

The network weights $\mathbf{W}$ are computed by an adaption law, which incorporates an adaptation gain $\Gamma > 0$ and an e-modification term $\mu > 0$[14] according to the update law

$$\dot{\mathbf{W}} = -\Gamma\left(\boldsymbol{\beta}\mathbf{e}^T\mathbf{P}\mathbf{B} + \mu\left\|\mathbf{e}^T\mathbf{P}\mathbf{B}\right\|\mathbf{W}\right) \tag{51}$$

where the matrix $\mathbf{P}$ solves the Lyapunov equation $\mathbf{A}^T\mathbf{P} + \mathbf{P}^T\mathbf{A} = -\mathbf{Q}$ for some positive-definite matrix $\mathbf{Q}$ and the norm is a Frobenius norm.

The e-modification term provides a robustness in the adaptation law.[14] The update law in Eq. (23) guarantees the stability of the network weights and the tracking error. The proof of this update law using the Lyapunov method is provided by Rysdyk and Calise.[11] Solving for the matrix $\mathbf{P}$ with $\mathbf{Q} = \mathbf{I}$, the update law can be rewritten as

$$\dot{\mathbf{W}} = -\Gamma \left(\boldsymbol{\beta} \mathbf{V} + \mu \left\| \mathbf{V} \right\| \mathbf{W} \right) \tag{52}$$

where

$$\mathbf{V} = \frac{1}{2} \boldsymbol{\omega}_e^T \mathbf{K}_p^{-1} \left(\mathbf{I} + \mathbf{K}_I^{-1} \right) + \frac{1}{2} \int_0^t \boldsymbol{\omega}_e^T d\tau \mathbf{K}_I^{-1} \tag{53}$$

VI. Hybrid Direct-Indirect Adaptive Control Concept

While the direct neural network adaptive law has been extensively research and has been used with good successes in a number of applications, the possibility of high gain control due to aggressive learning can be an issue. Aggressive learning is characterized by setting the learning rate Γ high enough so as to reduce the dynamic inversion error rapidly. This can potentially lead to a control augmentation command that may saturate the control authority. Moreover, high gain control may also excite unmodeled dynamics of the plant that can adversely affect the stability of the adaptive law. To address this issue, we are considering a modification to the present direct adaptive law to include an indirect adaptive law that provides an opportunity to perform an on-line estimation of the plant dynamics of the damaged aircraft explicitly. We call this approach as a hybrid direct-indirect adaptive control concept. The indirect adaptive law will provide an estimated plant dynamics that will be used in the dynamic inversion. If successful, the control command will result in a smaller dynamic inversion error so that the learning of the direct adaptation neural network can be reduced. An architecture of the proposed hybrid adaptive control concept is shown in Fig. 7. In the current study, we are developing some initial indirect adaptive laws for the on-line estimation of plant dynamics based on the Lyapunov stability theory and also the well-known recursive least-square method. Future research still remains ahead to rigorously investigate this proposed concept followed by high-fidelity simulations.
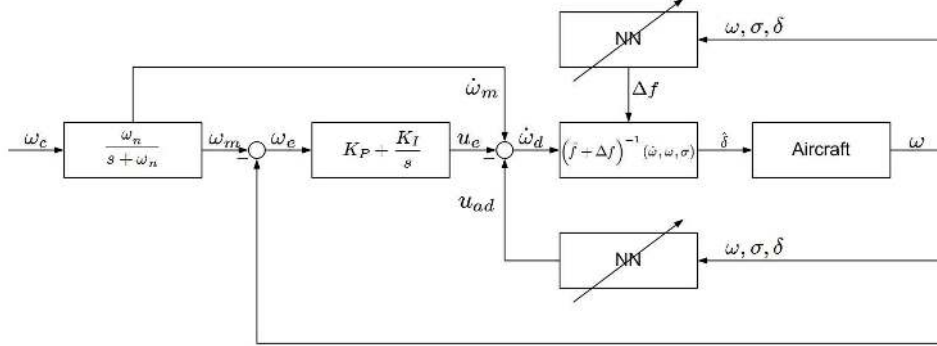
Fig. 7 - Hybrid Direct-Indirect Neural Network Adaptive Flight Control Architecture

A. Indirect Neural Network Adaptive Control

We would like to estimate the unknown plant matrices using a linear-in-parameter neural network approach as

$$\Delta \hat{\mathbf{F}}_1 = \mathbf{W}_{\boldsymbol{\omega}}^T \boldsymbol{\beta}_{\boldsymbol{\omega}} \tag{54}$$

$$\Delta \hat{\mathbf{F}}_2 = \mathbf{W}_{\boldsymbol{\sigma}}^T \boldsymbol{\beta}_{\boldsymbol{\sigma}} \tag{55}$$

$$\Delta \hat{\mathbf{G}} = \mathbf{W}_{\boldsymbol{\delta}}^T \boldsymbol{\beta}_{\boldsymbol{\delta}} \tag{56}$$

where the hat symbol denotes the estimated plant matrices and $\boldsymbol{\beta}_{\boldsymbol{\omega}}, \boldsymbol{\beta}_{\boldsymbol{\sigma}}, \boldsymbol{\beta}_{\boldsymbol{\delta}}$ are some neural network architectures that may not be necessarily the same as $\boldsymbol{\beta}$ for the direct adaptation neural network.

The error dynamics now can be expressed as

$$\dot{\mathbf{e}} = \mathbf{A}\mathbf{e} + \mathbf{B}\mathbf{W}^T \boldsymbol{\beta} - \mathbf{B}\mathbf{W}_{\boldsymbol{\omega}}^T \boldsymbol{\beta}_{\boldsymbol{\omega}} \tilde{\boldsymbol{\omega}} - \mathbf{B}\mathbf{W}_{\boldsymbol{\sigma}}^T \boldsymbol{\beta}_{\boldsymbol{\sigma}} \boldsymbol{\sigma} - \mathbf{B}\mathbf{W}_{\boldsymbol{\delta}}^T \boldsymbol{\beta}_{\boldsymbol{\delta}} \hat{\boldsymbol{\delta}} - \mathbf{B}\Delta\varepsilon \tag{57}$$

where $\Delta\varepsilon < \varepsilon$ is the residual error from the estimation of the plant matrices.

We now propose the following adaptive laws for the estimation of $\mathbf{W}_{\boldsymbol{\omega}}$, $\mathbf{W}_{\boldsymbol{\sigma}}$, and $\mathbf{W}_{\boldsymbol{\delta}}$

$$\dot{\mathbf{W}}_{\boldsymbol{\omega}} = \Gamma_{\boldsymbol{\omega}}\boldsymbol{\beta}_{\boldsymbol{\omega}}\tilde{\boldsymbol{\omega}}\mathbf{e}^T\mathbf{PB} \tag{58}$$

$$\dot{\mathbf{W}}_{\boldsymbol{\sigma}} = \Gamma_{\boldsymbol{\sigma}}\boldsymbol{\beta}_{\boldsymbol{\sigma}}\boldsymbol{\sigma}\mathbf{e}^T\mathbf{PB} \tag{59}$$

$$\dot{\mathbf{W}}_{\boldsymbol{\delta}} = \Gamma_{\boldsymbol{\delta}}\boldsymbol{\beta}_{\boldsymbol{\delta}}\hat{\boldsymbol{\delta}}\mathbf{e}^T\mathbf{PB} \tag{60}$$

where $\Gamma_{\boldsymbol{\omega}}, \Gamma_{\boldsymbol{\sigma}}, \Gamma_{\boldsymbol{\delta}} > 0$ are the adaptation gains.

The proof is as follows:

We assume $\dot{\mathbf{e}}, \tilde{\boldsymbol{\omega}}, \boldsymbol{\sigma}, \hat{\boldsymbol{\delta}} \in \mathcal{L}_\infty$. We then let $\mathbf{W} = \mathbf{W}^* + \tilde{\mathbf{W}}$, $\mathbf{W}_{\boldsymbol{\omega}} = \mathbf{W}_{\boldsymbol{\omega}}^* + \tilde{\mathbf{W}}_{\boldsymbol{\omega}}$, $\mathbf{W}_{\boldsymbol{\sigma}} = \mathbf{W}_{\boldsymbol{\sigma}}^* + \tilde{\mathbf{W}}_{\boldsymbol{\sigma}}$, and $\mathbf{W}_{\boldsymbol{\delta}} = \mathbf{W}_{\boldsymbol{\delta}}^* + \tilde{\mathbf{W}}_{\boldsymbol{\delta}}$ where the asterisk symbol denotes the ideal weight matrices to cancel out the residual error $\Delta\varepsilon$ and the tilde symbol denotes the weight deviations.

The ideal weight matrices are unknown but they may be assumed constant and bounded to stay within a $\boldsymbol{\Delta}$-neighborhood of the residual error $\Delta\varepsilon$ so that

$$\boldsymbol{\Delta} = \sup_{\boldsymbol{\omega},\boldsymbol{\sigma},\hat{\boldsymbol{\delta}}} \left\| \mathbf{W}^{*T}\boldsymbol{\beta} - \mathbf{W}_{\boldsymbol{\omega}}^{*T}\boldsymbol{\beta}_{\boldsymbol{\omega}}\tilde{\boldsymbol{\omega}} - \mathbf{W}_{\boldsymbol{\sigma}}^{*T}\boldsymbol{\beta}_{\boldsymbol{\sigma}}\boldsymbol{\sigma} - \mathbf{W}_{\boldsymbol{\delta}}^{*T}\boldsymbol{\beta}_{\boldsymbol{\delta}}\hat{\boldsymbol{\delta}} - \Delta\varepsilon \right\| \tag{61}$$

We define the following Lyapunov function

$$V = \mathbf{e}^T\mathbf{Pe} + \mathrm{tr}\left(\frac{\tilde{\mathbf{W}}^T\tilde{\mathbf{W}}}{\Gamma} + \frac{\tilde{\mathbf{W}}_{\boldsymbol{\omega}}^T\tilde{\mathbf{W}}_{\boldsymbol{\omega}}}{\Gamma_{\boldsymbol{\omega}}} + \frac{\tilde{\mathbf{W}}_{\boldsymbol{\sigma}}^T\tilde{\mathbf{W}}_{\boldsymbol{\sigma}}}{\Gamma_{\boldsymbol{\sigma}}} + \frac{\tilde{\mathbf{W}}_{\boldsymbol{\delta}}^T\tilde{\mathbf{W}}_{\boldsymbol{\delta}}}{\Gamma_{\boldsymbol{\delta}}} \right) \tag{62}$$

where $\mathbf{P} \geq \mathbf{0}$ and $\mathrm{tr}(\mathbf{A})$ denotes the trace of a matrix $\mathbf{A}$.

The time derivative of the Lyapunov function is computed as

$$\dot{V} = \dot{\mathbf{e}}^T\mathbf{Pe} + \mathbf{e}^T\mathbf{P}\dot{\mathbf{e}} + 2\mathrm{tr}\left(\frac{\tilde{\mathbf{W}}^T\dot{\tilde{\mathbf{W}}}}{\Gamma} + \frac{\tilde{\mathbf{W}}_{\boldsymbol{\omega}}^T\dot{\tilde{\mathbf{W}}}_{\boldsymbol{\omega}}}{\Gamma_{\boldsymbol{\omega}}} + \frac{\tilde{\mathbf{W}}_{\boldsymbol{\sigma}}^T\dot{\tilde{\mathbf{W}}}_{\boldsymbol{\sigma}}}{\Gamma_{\boldsymbol{\sigma}}} + \frac{\tilde{\mathbf{W}}_{\boldsymbol{\delta}}^T\dot{\tilde{\mathbf{W}}}_{\boldsymbol{\delta}}}{\Gamma_{\boldsymbol{\delta}}} \right) \tag{63}$$

Substituting Eqs. (57) and (51) into the above equation yields

$$\begin{aligned}
\dot{V} = &-\mathbf{e}^T\mathbf{Qe} + 2\mathbf{e}^T\mathbf{PB}\left(\mathbf{W}^{*T} + \tilde{\mathbf{W}}^T\right)\boldsymbol{\beta} - 2\mathbf{e}^T\mathbf{PB}\left(\mathbf{W}_{\boldsymbol{\omega}}^{*T} + \tilde{\mathbf{W}}_{\boldsymbol{\omega}}^T\right)\boldsymbol{\beta}_{\boldsymbol{\omega}}\tilde{\boldsymbol{\omega}} \\
&- 2\mathbf{e}^T\mathbf{PB}\left(\mathbf{W}_{\boldsymbol{\sigma}}^{*T} + \tilde{\mathbf{W}}_{\boldsymbol{\sigma}}^T\right)\boldsymbol{\beta}_{\boldsymbol{\sigma}}\boldsymbol{\sigma} - 2\mathbf{e}^T\mathbf{PB}\left(\mathbf{W}_{\boldsymbol{\delta}}^{*T} + \tilde{\mathbf{W}}_{\boldsymbol{\delta}}^T\right)\boldsymbol{\beta}_{\boldsymbol{\delta}}\hat{\boldsymbol{\delta}} - 2\mathbf{e}^T\mathbf{PB}\Delta\varepsilon \\
&+ 2\mathrm{tr}\left[-\tilde{\mathbf{W}}^T\boldsymbol{\beta}\mathbf{e}^T\mathbf{PB} - \mu\tilde{\mathbf{W}}^T\left\|\mathbf{e}^T\mathbf{PB}\right\|\left(\mathbf{W}^* + \tilde{\mathbf{W}}\right) + \frac{\tilde{\mathbf{W}}_{\boldsymbol{\omega}}^T\dot{\tilde{\mathbf{W}}}_{\boldsymbol{\omega}}}{\Gamma_{\boldsymbol{\omega}}} + \frac{\tilde{\mathbf{W}}_{\boldsymbol{\sigma}}^T\dot{\tilde{\mathbf{W}}}_{\boldsymbol{\sigma}}}{\Gamma_{\boldsymbol{\sigma}}} + \frac{\tilde{\mathbf{W}}_{\boldsymbol{\delta}}^T\dot{\tilde{\mathbf{W}}}_{\boldsymbol{\delta}}}{\Gamma_{\boldsymbol{\delta}}} \right] \tag{64}
\end{aligned}$$

We note that $\mathrm{tr}(\mathbf{AB}) = \mathrm{tr}(\mathbf{BA})$, so that

$$\mathbf{e}^T\mathbf{PB}\tilde{\mathbf{W}}^T\boldsymbol{\beta} = \mathrm{tr}\left(\mathbf{e}^T\mathbf{PB}\tilde{\mathbf{W}}^T\boldsymbol{\beta}\right) = \mathrm{tr}\left(\tilde{\mathbf{W}}^T\boldsymbol{\beta}\mathbf{e}^T\mathbf{PB}\right) \tag{65}$$

$$\mathbf{e}^T\mathbf{PB}\tilde{\mathbf{W}}_{\boldsymbol{\omega}}^T\boldsymbol{\beta}_{\boldsymbol{\omega}}\tilde{\boldsymbol{\omega}} = \mathrm{tr}\left(\mathbf{e}^T\mathbf{PB}\tilde{\mathbf{W}}_{\boldsymbol{\omega}}^T\boldsymbol{\beta}_{\boldsymbol{\omega}}\tilde{\boldsymbol{\omega}}\right) = \mathrm{tr}\left(\tilde{\mathbf{W}}_{\boldsymbol{\omega}}^T\boldsymbol{\beta}_{\boldsymbol{\omega}}\tilde{\boldsymbol{\omega}}\mathbf{e}^T\mathbf{PB}\right) \tag{66}$$

$$\mathbf{e}^T\mathbf{PB}\tilde{\mathbf{W}}_{\boldsymbol{\sigma}}^T\boldsymbol{\beta}_{\boldsymbol{\sigma}}\boldsymbol{\sigma} = \mathrm{tr}\left(\mathbf{e}^T\mathbf{PB}\tilde{\mathbf{W}}_{\boldsymbol{\sigma}}^T\boldsymbol{\beta}_{\boldsymbol{\sigma}}\boldsymbol{\sigma}\right) = \mathrm{tr}\left(\tilde{\mathbf{W}}_{\boldsymbol{\sigma}}^T\boldsymbol{\beta}_{\boldsymbol{\sigma}}\boldsymbol{\sigma}\mathbf{e}^T\mathbf{PB}\right) \tag{67}$$

$$\mathbf{e}^T\mathbf{PB}\tilde{\mathbf{W}}_{\boldsymbol{\delta}}^T\boldsymbol{\beta}_{\boldsymbol{\delta}}\hat{\boldsymbol{\delta}} = \mathrm{tr}\left(\mathbf{e}^T\mathbf{PB}\tilde{\mathbf{W}}_{\boldsymbol{\delta}}^T\boldsymbol{\beta}_{\boldsymbol{\delta}}\hat{\boldsymbol{\delta}}\right) = \mathrm{tr}\left(\tilde{\mathbf{W}}_{\boldsymbol{\delta}}^T\boldsymbol{\beta}_{\boldsymbol{\delta}}\hat{\boldsymbol{\delta}}\mathbf{e}^T\mathbf{PB}\right) \tag{68}$$

Also, by completing the square, we have

$$2\mathrm{tr}\left[-\mu\tilde{\mathbf{W}}^T\left\|\mathbf{e}^T\mathbf{PB}\right\|\left(\mathbf{W}^* + \tilde{\mathbf{W}}\right) \right] = -2\mu\left\|\mathbf{e}^T\mathbf{PB}\right\|\left(\left\|\frac{\mathbf{W}^*}{2} + \tilde{\mathbf{W}}\right\|^2 - \left\|\frac{\mathbf{W}^*}{2}\right\|^2 \right) \tag{69}$$

Since $\dot{\tilde{\mathbf{W}}}_{\boldsymbol{\omega}} = \dot{\mathbf{W}}_{\boldsymbol{\omega}}$, $\dot{\tilde{\mathbf{W}}}_{\boldsymbol{\sigma}} = \dot{\mathbf{W}}_{\boldsymbol{\sigma}}$, and $\dot{\tilde{\mathbf{W}}}_{\boldsymbol{\delta}} = \dot{\mathbf{W}}_{\boldsymbol{\delta}}$, Eq. (64) then becomes

$$\dot{V} \leq -\mathbf{e}^T \mathbf{Q}\mathbf{e} + 2\mathbf{e}^T \mathbf{P}\mathbf{B}\boldsymbol{\Delta} - 2\mu \left\|\mathbf{e}^T \mathbf{P}\mathbf{B}\right\| \left(\left\|\frac{\mathbf{W}^*}{2} + \tilde{\mathbf{W}}\right\|^2 - \left\|\frac{\mathbf{W}^*}{2}\right\|^2 \right)$$

$$2\text{tr}\left[\tilde{\mathbf{W}}_{\boldsymbol{\omega}}^T \left(\frac{\dot{\mathbf{W}}_{\boldsymbol{\omega}}}{\Gamma_{\boldsymbol{\omega}}} - \boldsymbol{\beta}_{\boldsymbol{\omega}}\tilde{\boldsymbol{\omega}}\mathbf{e}^T \mathbf{P}\mathbf{B} \right) + \tilde{\mathbf{W}}_{\boldsymbol{\sigma}}^T \left(\frac{\dot{\mathbf{W}}_{\boldsymbol{\sigma}}}{\Gamma_{\boldsymbol{\sigma}}} - \boldsymbol{\beta}_{\boldsymbol{\sigma}}\boldsymbol{\sigma}\mathbf{e}^T \mathbf{P}\mathbf{B} \right) + \tilde{\mathbf{W}}_{\boldsymbol{\delta}}^T \left(\frac{\dot{\mathbf{W}}_{\boldsymbol{\delta}}}{\Gamma_{\boldsymbol{\delta}}} - \boldsymbol{\beta}_{\boldsymbol{\delta}}\hat{\boldsymbol{\delta}}\mathbf{e}^T \mathbf{P}\mathbf{B} \right) \right] \quad (70)$$

Since $\|\mathbf{B}\| = 1$, we establish that

$$\mathbf{e}^T \mathbf{Q}\mathbf{e} \leq \rho\left(\mathbf{Q}\right) \|\mathbf{e}\|^2 \tag{71}$$

$$\mathbf{e}^T \mathbf{P}\mathbf{B}\boldsymbol{\Delta} \leq \rho\left(\mathbf{P}\right) \|\mathbf{e}\| \|\boldsymbol{\Delta}\| \tag{72}$$

$$\left\|\mathbf{e}^T \mathbf{P}\mathbf{B}\right\| \left\|\frac{\mathbf{W}^*}{2}\right\|^2 \leq \rho\left(\mathbf{P}\right) \|\mathbf{e}\| \left\|\frac{\mathbf{W}^*}{2}\right\|^2 \tag{73}$$

where $\rho\left(\mathbf{Q}\right)$ and $\rho\left(\mathbf{P}\right)$ are the spectral radii of $\mathbf{Q}$ and $\mathbf{P}$.

In order to guarantee that $\dot{V} \leq 0$, we require that the trace operator be equal to zero, thus resulting in the adaptive laws in Eqs. (58) to (60). In addition, we also require that

$$\|\mathbf{e}\| > \frac{\rho\left(\mathbf{P}\right)}{2\rho\left(\mathbf{Q}\right)} \left(4\|\boldsymbol{\Delta}\| + \mu\|\mathbf{W}^*\|^2 \right) \tag{74}$$

The time rate of change of the Lyapunov function is then strictly negative and therefore it would guarantee that the signals are bounded. We note that $\dot{\mathbf{e}}, \tilde{\boldsymbol{\omega}}, \boldsymbol{\sigma}, \hat{\boldsymbol{\delta}} \in \mathcal{L}_\infty$ but $\mathbf{e} \in \mathcal{L}_2$ since

$$\int_0^\infty \mathbf{e}^T \mathbf{Q}\mathbf{e}\,dt \leq \rho\left(\mathbf{Q}\right) \int_0^\infty \|\mathbf{e}\|^2\,dt \leq V(0) - V(t \to \infty) + 2\rho\left(\mathbf{P}\right) \int_0^\infty \|\mathbf{e}\| \|\boldsymbol{\Delta}\|\,dt$$

$$- 2\mu\rho\left(\mathbf{P}\right) \int_0^\infty \|\mathbf{e}\| \left(\left\|\frac{\mathbf{W}^*}{2} + \tilde{\mathbf{W}}\right\|^2 - \left\|\frac{\mathbf{W}^*}{2}\right\|^2 \right) dt < \infty \quad (75)$$

Utilizing Eq. (74), we have

$$V(t \to \infty) \leq V(0) - 2\mu\rho\left(\mathbf{P}\right) \int_0^\infty \|\mathbf{e}\| \left\|\frac{\mathbf{W}^*}{2} + \tilde{\mathbf{W}}\right\|^2 dt < \infty \tag{76}$$

Thus, the value of V as $t \to \infty$ is bounded. Therefore, we establish that $\left\|\dot{\mathbf{W}}\right\| \to \mathbf{0}$, $\left\|\dot{\mathbf{W}}_{\boldsymbol{\omega}}\right\| \to \mathbf{0}$, $\left\|\dot{\mathbf{W}}_{\boldsymbol{\sigma}}\right\| \to \mathbf{0}$, and $\left\|\dot{\mathbf{W}}_{\boldsymbol{\delta}}\right\| \to \mathbf{0}$ imply $\|\mathbf{e}\| \to \mathbf{0}$ as $t \to \infty$. This means that the adaptive laws will result in a convergence of the estimated $\Delta\mathbf{F}_1$, $\Delta\mathbf{F}_2$, and $\Delta\mathbf{G}$ to their steady state values. In practice, the inputs $\boldsymbol{\phi} = \begin{bmatrix} \tilde{\boldsymbol{\omega}}^T & \boldsymbol{\sigma}^T & \hat{\boldsymbol{\delta}}^T \end{bmatrix}^T$ must be sufficiently rich that contain enough frequencies to capture all the plant dynamics. In order for the on-line estimation to converge the their correct values, the inputs need to be a persistent excitation (PE) class of signals such that if there exist $\alpha_0, \alpha_1, T_0 > 0$ then[9]

$$\alpha_0 \mathbf{I} \leq \int_t^{t+T_0} \boldsymbol{\phi}(\tau)\boldsymbol{\phi}^T(\tau)\,d\tau \leq \alpha_1 \mathbf{I} \tag{77}$$

We can also "robustify" the adaptive laws similar to Eq. (52) to better handle unmodeled dynamics and disturbances by adding an e-modification term[14] to Eqs. (58) to (60) as

$$\dot{\mathbf{W}}_{\boldsymbol{\omega}} = \Gamma_{\boldsymbol{\omega}} \left(\boldsymbol{\beta}_{\boldsymbol{\omega}}\tilde{\boldsymbol{\omega}}\mathbf{e}^T \mathbf{P}\mathbf{B} - \mu_{\boldsymbol{\omega}} \left\|\mathbf{e}^T \mathbf{P}\mathbf{B}\right\| \mathbf{W}_{\boldsymbol{\omega}} \right) \tag{78}$$

$$\dot{\mathbf{W}}_{\boldsymbol{\sigma}} = \Gamma_{\boldsymbol{\sigma}} \left(\boldsymbol{\beta}_{\boldsymbol{\sigma}}\boldsymbol{\sigma}\mathbf{e}^T \mathbf{P}\mathbf{B} - \mu_{\boldsymbol{\sigma}} \left\|\mathbf{e}^T \mathbf{P}\mathbf{B}\right\| \mathbf{W}_{\boldsymbol{\sigma}} \right) \tag{79}$$

$$\dot{\mathbf{W}}_{\boldsymbol{\delta}} = \Gamma_{\boldsymbol{\delta}} \left(\boldsymbol{\beta}_{\boldsymbol{\delta}}\hat{\boldsymbol{\delta}}\mathbf{e}^T \mathbf{P}\mathbf{B} - \mu_{\boldsymbol{\delta}} \left\|\mathbf{e}^T \mathbf{P}\mathbf{B}\right\| \mathbf{W}_{\boldsymbol{\delta}} \right) \tag{80}$$

in which case the time rate of change of the Lyapunov function becomes

$$\dot{V} \le -2\mu \left\| \mathbf{e}^T \mathbf{PB} \right\| \left\| \frac{\mathbf{W}^*}{2} + \tilde{\mathbf{W}} \right\|^2 - 2\mu_{\boldsymbol{\omega}} \left\| \mathbf{e}^T \mathbf{PB} \right\| \left\| \frac{\tilde{\mathbf{W}}_{\boldsymbol{\omega}}^*}{2} + \tilde{\mathbf{W}}_{\boldsymbol{\omega}} \right\|^2$$

$$- 2\mu_{\boldsymbol{\sigma}} \left\| \mathbf{e}^T \mathbf{PB} \right\| \left\| \frac{\tilde{\mathbf{W}}_{\boldsymbol{\sigma}}^*}{2} + \tilde{\mathbf{W}}_{\boldsymbol{\sigma}} \right\|^2 - 2\mu_{\boldsymbol{\delta}} \left\| \mathbf{e}^T \mathbf{PB} \right\| \left\| \frac{\tilde{\mathbf{W}}_{\boldsymbol{\delta}}^*}{2} + \tilde{\mathbf{W}}_{\boldsymbol{\delta}} \right\|^2 \quad (81)$$

The effect of the e-modification is to increase the negative time rate of change of the Lyapunov function so that as long as the effects of unmodeled dynamics and or disturbances do not exceed the value of $\dot{V}$, the adaptive signals should remain bounded. The e-modification thus makes the adaptive law robust to unmodeled dynamics so that the PE condition may not be needed.[15]

It should be noted that we have so far assumed that $\tilde{\boldsymbol{\omega}}, \boldsymbol{\sigma}, \hat{\boldsymbol{\delta}} \in \mathcal{L}_\infty$. Suppose that $\tilde{\boldsymbol{\omega}}, \boldsymbol{\sigma}, \hat{\boldsymbol{\delta}} \notin \mathcal{L}_\infty$, the adaptive laws in Eqs. (58) to (60) will become unstable because $\tilde{\boldsymbol{\omega}}, \boldsymbol{\sigma}$, and $\hat{\boldsymbol{\delta}}$ are unbounded. Therefore, we must modify the adaptive laws to handle unbounded signals by a normalization method.[9] We note that $\tilde{\boldsymbol{\omega}} \left(1 + \tilde{\boldsymbol{\omega}}^T \tilde{\boldsymbol{\omega}} \right)^{-1} \in \mathcal{L}_\infty$ since

$$\lim_{\tilde{\boldsymbol{\omega}} \to \infty} \frac{\tilde{\boldsymbol{\omega}}}{1 + \tilde{\boldsymbol{\omega}}^T \tilde{\boldsymbol{\omega}}} = 0 \quad (82)$$

Therefore, the normalized adaptive laws for unbounded signals should be

$$\dot{\mathbf{W}}_{\boldsymbol{\omega}} = \Gamma_{\boldsymbol{\omega}} \left(1 + \tilde{\boldsymbol{\omega}}^T \tilde{\boldsymbol{\omega}} \right)^{-1} \left(\boldsymbol{\beta}_{\boldsymbol{\omega}} \tilde{\boldsymbol{\omega}} \mathbf{e}^T \mathbf{PB} - \mu_{\boldsymbol{\omega}} \left\| \mathbf{e}^T \mathbf{PB} \right\| \mathbf{W}_{\boldsymbol{\omega}} \right) \quad (83)$$

$$\dot{\mathbf{W}}_{\boldsymbol{\sigma}} = \Gamma_{\boldsymbol{\sigma}} \left(1 + \boldsymbol{\sigma}^T \boldsymbol{\sigma} \right)^{-1} \left(\boldsymbol{\beta}_{\boldsymbol{\sigma}} \boldsymbol{\sigma} \mathbf{e}^T \mathbf{PB} - \mu_{\boldsymbol{\sigma}} \left\| \mathbf{e}^T \mathbf{PB} \right\| \mathbf{W}_{\boldsymbol{\sigma}} \right) \quad (84)$$

$$\dot{\mathbf{W}}_{\boldsymbol{\delta}} = \Gamma_{\boldsymbol{\delta}} \left(1 + \hat{\boldsymbol{\delta}}^T \hat{\boldsymbol{\delta}} \right)^{-1} \left(\boldsymbol{\beta}_{\boldsymbol{\delta}} \hat{\boldsymbol{\delta}} \mathbf{e}^T \mathbf{PB} - \mu_{\boldsymbol{\delta}} \left\| \mathbf{e}^T \mathbf{PB} \right\| \mathbf{W}_{\boldsymbol{\delta}} \right) \quad (85)$$

B. Recursive Least-Square Parameter Identification

While the indirect adaptive laws above provide a computational method for on-line estimation of the plant dynamics, it would be incomplete to not consider the well-known least-square method which is equally robust in parameter identification process. If the dynamic inversion error is somehow can be estimated, then we should be able to apply a recursive least-square method to determine the weight matrices $\mathbf{W}_{\boldsymbol{\omega}}, \mathbf{W}_{\boldsymbol{\sigma}}$, and $\mathbf{W}_{\boldsymbol{\delta}}$. Suppose the estimated dynamic inversion error can be written as

$$\boldsymbol{\varepsilon} = \boldsymbol{\Phi}^T \boldsymbol{\theta} + \Delta \boldsymbol{\varepsilon} \quad (86)$$

where $\boldsymbol{\Phi}^T = \begin{bmatrix} \mathbf{W}_{\boldsymbol{\omega}}^T & \mathbf{W}_{\boldsymbol{\sigma}}^T & \mathbf{W}_{\boldsymbol{\delta}}^T \end{bmatrix}$, $\boldsymbol{\theta} = \begin{bmatrix} \boldsymbol{\beta}_{\boldsymbol{\omega}} \tilde{\boldsymbol{\omega}} & \boldsymbol{\beta}_{\boldsymbol{\sigma}} \boldsymbol{\sigma} & \boldsymbol{\beta}_{\boldsymbol{\delta}} \hat{\boldsymbol{\delta}} \end{bmatrix}^T$, and $\Delta \boldsymbol{\varepsilon}$ is the computational error in the estimated dynamic inversion error $\boldsymbol{\varepsilon}$, which may contain noise resulting from the on-line derivative computation of $\tilde{\boldsymbol{\omega}}$ since

$$\hat{\boldsymbol{\varepsilon}} = \dot{\hat{\boldsymbol{\omega}}} - \mathbf{F}_1 \tilde{\boldsymbol{\omega}} - \mathbf{F}_2 \boldsymbol{\sigma} - \mathbf{G} \hat{\boldsymbol{\delta}} \quad (87)$$

where $\dot{\hat{\boldsymbol{\omega}}}$ is the estimated angular acceleration which may be subject to computational errors.

One method of computing $\dot{\hat{\boldsymbol{\omega}}}$ is to use a backward finite-difference method

$$\dot{\hat{\boldsymbol{\omega}}}_i = \frac{\tilde{\boldsymbol{\omega}}_i - \tilde{\boldsymbol{\omega}}_{i-1}}{\Delta t} \quad (88)$$

to estimate $\dot{\hat{\boldsymbol{\omega}}}$ at the i-th time step, but this method can result in a significant error if Δt is either too small or too large.

Another approach is to collect n number of data points which will be used to generate an at least C^1 smooth curve in time using a cubic or B-spline method. This curve is then differentiated at their knots to find the estimated derivative values. In either case, the derivative computation will introduce an error source $\Delta \boldsymbol{\varepsilon}$. If the error is unbiased, i.e., it can be characterized as a white noise about the mean value, then the least-square method can be applied to estimate the plant dynamics.

We consider a minimization of the following cost function

$$J\left(\mathbf{W}_{\boldsymbol{\omega}}, \mathbf{W}_{\boldsymbol{\sigma}}, \mathbf{W}_{\boldsymbol{\delta}}\right) = \int_0^t \left\|\hat{\boldsymbol{\varepsilon}} - \boldsymbol{\Phi}^T \boldsymbol{\theta}\right\|^2 d\tau \tag{89}$$

Our objective is to find recursive least-square adaptive laws for $\mathbf{W}_{\boldsymbol{\omega}}$, $\mathbf{W}_{\boldsymbol{\sigma}}$, and $\mathbf{W}_{\boldsymbol{\delta}}$. To minimize the cost function, we compute the gradients with respects to the weight matrices, thus resulting in

$$\frac{\partial J}{\partial \boldsymbol{\Phi}}^T = -\int_0^t \boldsymbol{\theta}\left(\hat{\boldsymbol{\varepsilon}} - \boldsymbol{\Phi}^T \boldsymbol{\theta}\right)^T d\tau = \mathbf{0} \tag{90}$$

The recursive least-square formula using the gradient method is

$$\dot{\boldsymbol{\Phi}} = \mathbf{R}\boldsymbol{\theta}\left(\hat{\boldsymbol{\varepsilon}}^T - \boldsymbol{\theta}^T \boldsymbol{\Phi}\right) \tag{91}$$

where

$$\dot{\mathbf{R}} = -\mathbf{R}\boldsymbol{\theta}\boldsymbol{\theta}^T \mathbf{R} \tag{92}$$

To show this, we see that from Eq. (90)

$$\int_0^t \boldsymbol{\theta}\boldsymbol{\theta}^T d\tau \boldsymbol{\Phi} = \int_0^t \boldsymbol{\theta}\hat{\boldsymbol{\varepsilon}}^T d\tau \tag{93}$$

Let

$$\mathbf{R}^{-1} = \int_0^t \boldsymbol{\theta}\boldsymbol{\theta}^T d\tau > 0 \tag{94}$$

Then, differentiating Eqs. (93) and (94) results in

$$\mathbf{R}^{-1}\dot{\boldsymbol{\Phi}} + \dot{\mathbf{R}}^{-1}\boldsymbol{\Phi} = \boldsymbol{\theta}\hat{\boldsymbol{\varepsilon}}^T \tag{95}$$

$$\dot{\mathbf{R}}^{-1} = \boldsymbol{\theta}\boldsymbol{\theta}^T \tag{96}$$

Also, we have

$$\mathbf{R}\mathbf{R}^{-1} = \mathbf{I} \Rightarrow \dot{\mathbf{R}}\mathbf{R}^{-1} + \mathbf{R}\dot{\mathbf{R}}^{-1} = \mathbf{0} \tag{97}$$

Substituting Eq. (96) into Eqs. (95) and (96) and solving for $\dot{\boldsymbol{\Phi}}$ and $\dot{\mathbf{R}}$ yield the recursive least-square adaptive law. The matrix $\mathbf{R}$ is called the covariance matrix and the recursive least-square formula has a very similar form to the Kalman filter where Eq. (92) is a differential Riccati equation for a zero-order plant dynamics. We will show that the recursive weight update law is stable and results in bounded signals as follows:

We let $\boldsymbol{\Phi} = \boldsymbol{\Phi}^* + \tilde{\boldsymbol{\Phi}}$ with the hat and tilde symbols denoting ideal weights and weight deviations, respectively. Then, the error dynamics can be written as

$$\dot{\mathbf{e}} \leq \mathbf{A}\mathbf{e} + \mathbf{B}\tilde{\mathbf{W}}^T \boldsymbol{\beta} - \mathbf{B}\tilde{\boldsymbol{\Phi}}^T \boldsymbol{\theta} + \mathbf{B}\boldsymbol{\Delta} \tag{98}$$

We choose the following Lyapunov function

$$L = V + \text{tr}\left(\tilde{\boldsymbol{\Phi}}^T \mathbf{R}^{-1} \tilde{\boldsymbol{\Phi}}\right) \tag{99}$$

where V is the Lyapunov function for the direct neural network adaptive control and we have established that $\dot{V} \leq 0$.

The time rate of change of the Lyapunov function is computed as

$$\dot{L} = \dot{V} + \text{tr}\left(2\tilde{\boldsymbol{\Phi}}^T \mathbf{R}^{-1}\dot{\tilde{\boldsymbol{\Phi}}} + \tilde{\boldsymbol{\Phi}}^T \dot{\mathbf{R}}^{-1}\tilde{\boldsymbol{\Phi}}\right) \tag{100}$$

The weights $\boldsymbol{\Phi}$ can be shown to converge to the ideal weights $\boldsymbol{\Phi}^{*9}$ so that

$$\dot{\tilde{\boldsymbol{\Phi}}} = -\mathbf{R}\boldsymbol{\theta}\boldsymbol{\theta}^T \tilde{\boldsymbol{\Phi}} \tag{101}$$

Substituting Eq. (101) into Eq. (100) results in

$$\dot{L} = \dot{V} - \tilde{\mathbf{\Phi}}^T \boldsymbol{\theta}\boldsymbol{\theta}^T \tilde{\mathbf{\Phi}} \leq 0 \tag{102}$$

Thus, the recursive least square weight update law is stable.

In practice, the recursive least-square method can be used to estimate the plant dynamics either continuously or discretely at every n data samples. Continuous time estimation requires solving the differential equations (91) and (92) at each time step. On the other hands, the discrete-time sampling estimation provides more flexibility in that the estimation can be executed after a specified number of data points have been collected. This would ensure that the signals contained in the sampled data are sufficiently rich to enable an accurate convergence. Another advantage of the recursive least-square method is that it provides an optimal noise filtering to minimize noise effects in the estimation of the plant dynamics. The discrete-time recursive least square formula is

$$\mathbf{\Phi}_k = \mathbf{\Phi}_{k-1} + \mathbf{R}_{k-1}\boldsymbol{\theta}_k \left[\hat{\boldsymbol{\varepsilon}}_k^T - \boldsymbol{\theta}_k^T \mathbf{\Phi}_{k-1} \right] \tag{103}$$

$$\mathbf{R}_k = \mathbf{R}_{k-1} - \lambda^{-1}\mathbf{R}_{k-1}\boldsymbol{\theta}_k \left(\mathbf{I} + \lambda^{-1}\boldsymbol{\theta}_k^T \mathbf{R}_{k-1}\boldsymbol{\theta}_k \right)^{-1} \boldsymbol{\theta}_k^T \mathbf{R}_{k-1} \tag{104}$$

where k denotes the update cycle that repeats every n data samples, $\mathbf{\Phi}_k^T = \begin{bmatrix} \mathbf{W}_{\boldsymbol{\omega},k}^T & \mathbf{W}_{\boldsymbol{\sigma},k}^T & \mathbf{W}_{\boldsymbol{\delta},k}^T \end{bmatrix}^T$ is the weight matrix at k-th update cycle, λ is a forgetting factor that can be used to discount past data, and

$$\hat{\boldsymbol{\varepsilon}}_k^T = \begin{bmatrix} \hat{\boldsymbol{\omega}}_{kn-n+1}^T - \tilde{\boldsymbol{\omega}}_{kn-n+1}^T\mathbf{F}_1^T - \boldsymbol{\sigma}_{kn-n+1}^T\mathbf{F}_2^T - \hat{\boldsymbol{\delta}}_{kn-n+1}^T\mathbf{G}^T \\ \hat{\boldsymbol{\omega}}_{kn-n+2}^T - \tilde{\boldsymbol{\omega}}_{kn-n+2}^T\mathbf{F}_1^T - \boldsymbol{\sigma}_{kn-n+2}^T\mathbf{F}_2^T - \hat{\boldsymbol{\delta}}_{kn-n+2}^T\mathbf{G}^T \\ \vdots \\ \hat{\boldsymbol{\omega}}_{kn}^T - \tilde{\boldsymbol{\omega}}_{kn}^T\mathbf{F}_1^T - \boldsymbol{\sigma}_{kn}^T\mathbf{F}_2^T - \hat{\boldsymbol{\delta}}_{kn}^T\mathbf{G}^T \end{bmatrix} \tag{105}$$

$$\boldsymbol{\theta}_k^T = \begin{bmatrix} \tilde{\boldsymbol{\omega}}_{kn-n+1}^T\boldsymbol{\beta}_{\boldsymbol{\omega}}^T & \boldsymbol{\sigma}_{kn-n+1}^T\boldsymbol{\beta}_{\boldsymbol{\sigma}}^T & \hat{\boldsymbol{\delta}}_{kn-n+1}^T\boldsymbol{\beta}_{\boldsymbol{\delta}}^T \\ \tilde{\boldsymbol{\omega}}_{kn-n+2}^T\boldsymbol{\beta}_{\boldsymbol{\omega}}^T & \boldsymbol{\sigma}_{kn-n+2}^T\boldsymbol{\beta}_{\boldsymbol{\sigma}}^T & \hat{\boldsymbol{\delta}}_{kn-n+2}^T\boldsymbol{\beta}_{\boldsymbol{\delta}}^T \\ \vdots & \vdots & \vdots \\ \tilde{\boldsymbol{\omega}}_{kn}^T\boldsymbol{\beta}_{\boldsymbol{\omega}}^T & \boldsymbol{\sigma}_{kn}^T\boldsymbol{\beta}_{\boldsymbol{\sigma}}^T & \hat{\boldsymbol{\delta}}_{kn}^T\boldsymbol{\beta}_{\boldsymbol{\delta}}^T \end{bmatrix} \tag{106}$$

VII. Control Simulations

The neural network adaptive flight control for damaged aircraft is evaluated in a medium-fidelity simulation test environment. The flight simulator is a fixed-motion simulator equipped with a pilot station, programmable displays, and a 120º field-of-view visual system as shown in Fig. 8. Pilot command inputs are received through a control stick, a rudder pedal, and a throttle quadrant. Flight control software includes a flight dynamics model of damaged aircraft as developed herein. Simulations are performed at a 30 Hz frequency.

The damaged GTM is evaluated with various wing loss configurations. Fig. 9 shows the angular rates of the damaged GTM with and without the neural network adaptive flight control. The neural network control augmentation can be seen to quickly adapt to the changing dynamics of the damaged GTM. The roll, pitch, and yaw rates are quickly brought to zero to stabilize the damaged aircraft. In contrast, without a neural network control augmentation, the aircraft rates are changing rapidly, particularly in the roll axis. A rapid increase in the pitch attitude can result in the damaged GTM reaching its stall angle of attack that would render the aircraft in a dangerous situation.

Fig. 10 shows the control surface deflections corresponding to the neural network control augmentation. The right aileron is commanded to move substantially to correct for a left turning rolling moment resulting from a left wing damage. A maximum aileron limit of 35º is nearly reached. Thus, it is possible that for certain damage scenarios, the control augmentation will not be able to stabilize the damaged aircraft due to the control power limitation. In such situations, other types of control surfaces must be considered to provide additional control authorities for stabilization. Optimal control allocation approach must be incorporated into the neural network adaptive flight control to maximize the control effectiveness of all the available control authorities.
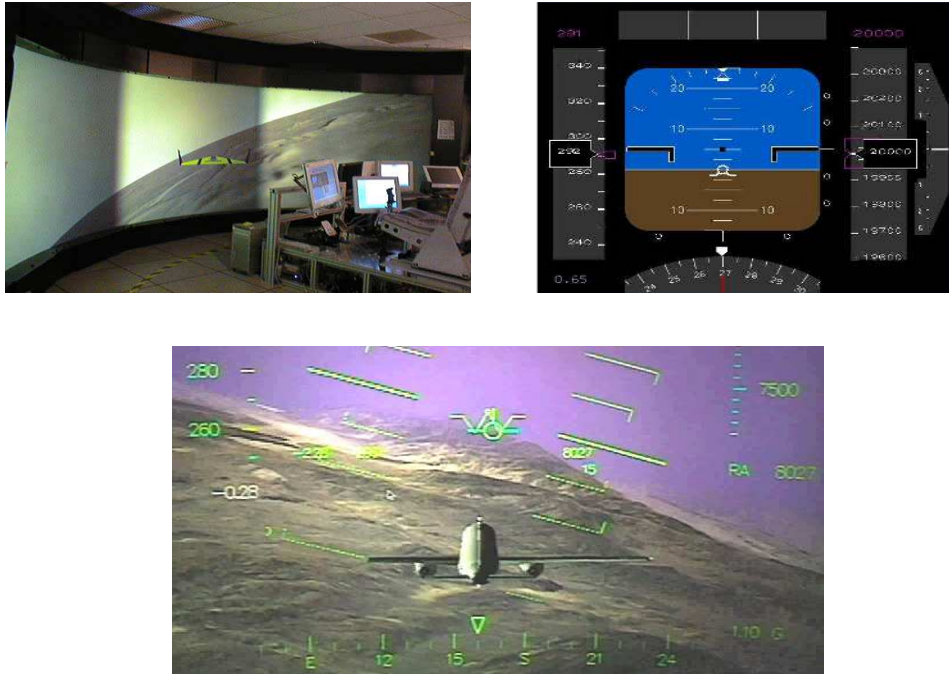
American Institute of Aeronautics and Astronautics

Fig. 8 - Flight Simulation Test Environment
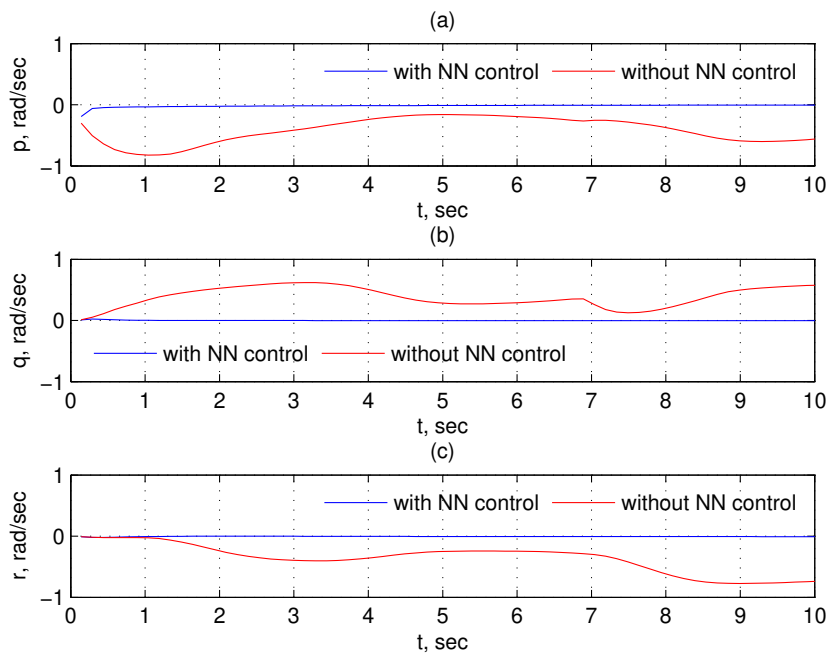
Fig. 9 - Rate Control with and without Neural Network Adaptation

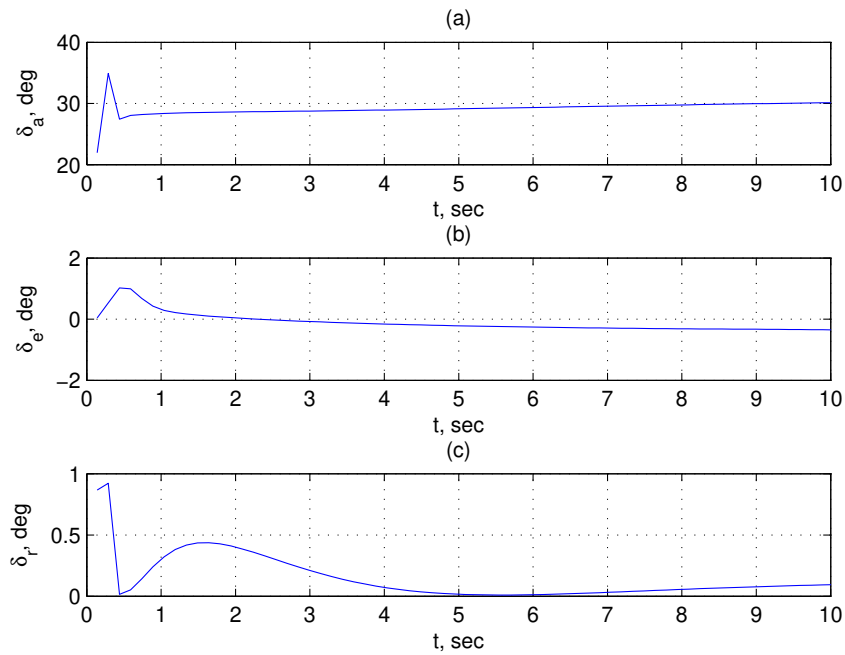American Institute of Aeronautics and Astronautics

Fig. 10 - Control Surface Deflection

To evaluate the hybrid adaptive flight control with the indirect adaptive law and the recursive least square method, a simulation was performed in MATLAB environment. A damage configuration corresponding to a 30% loss of the left wing is selected. A step input pitch doublet is simulated. The tracking performance of the three control laws is compared in Fig. 11.
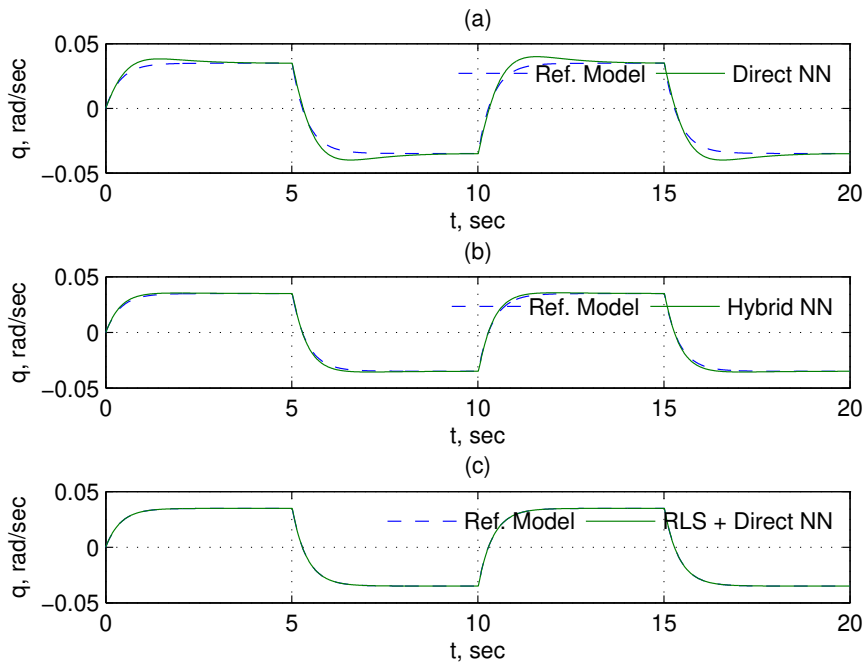
Fig. 11 - Pitch Doublet Tracking Performance

American Institute of Aeronautics and Astronautics
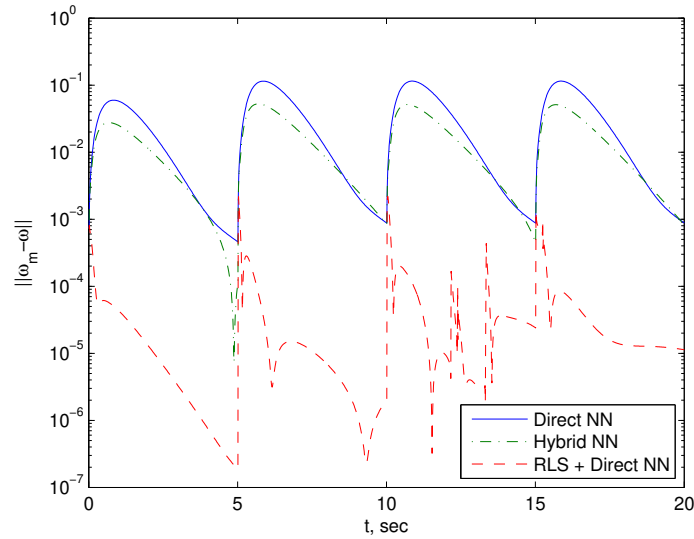
Fig. 12 - Tracking Error Norm

As can be seen, the hybrid adaptive control with the indirect adaptive law is able to improve the tracking performance of the direct neural network adaptive control. The combined direct adaptive control with the recursive least square parameter identification actually outperforms both the direct and hybrid adaptive control approaches as the tracking error is significantly reduced as seen in Fig. 12. The control surface deflections to achieve this pitch maneuver are shown in Fig. 13. The elevator deflection for this pitch maneuver is nearly saturated. The direct neural network adaptive control produces more overshoot than the hybrid adaptive control and the recursive least square approach. The left rolling moment is compensated by the right aileron input and the adverse yaw is compensated by a small rudder input. For this simulation, the actuator dynamics is not included in the study.

Fig. 13 - Control Surface Deflection

American Institute of Aeronautics and Astronautics
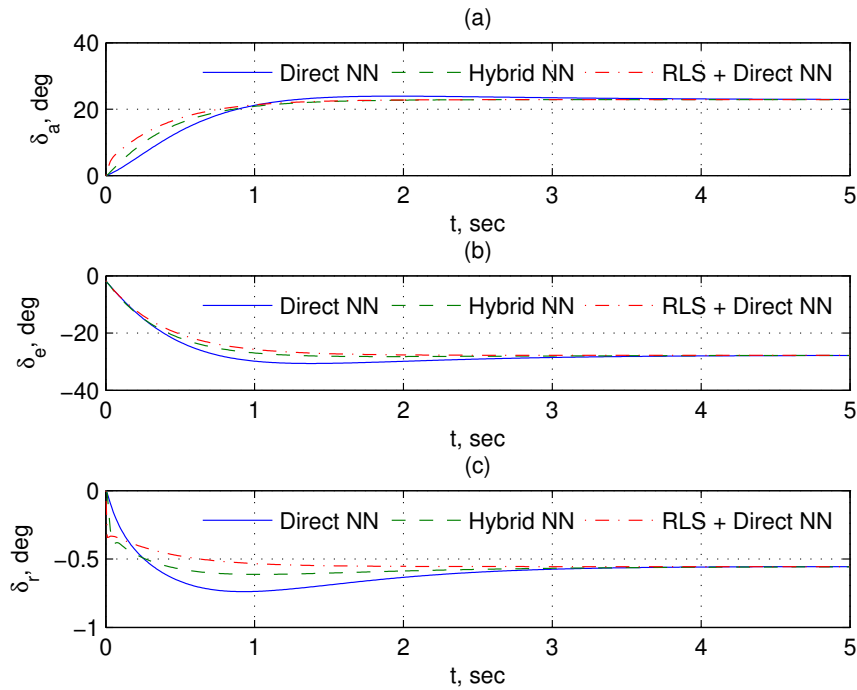
VIII. Discussions

The current research in the damage effect aerodynamic modeling has focused on single damage sites. Multiple damage sites can also exist in a damage event. The next step in damage effect aerodynamic modeling is to generate a predictive capability for multiple damage sites. An approach would be to conduct CFD modeling for representative multiple damage patterns. These modeling results are compared to single damage site models and a learning system can be developed to establish a surface response mapping between multiple and single damage sites. Using this damage surface response mapping, damage effects for any arbitrary damage pattern can be rapidly estimated.

In the current adaptive flight control research, only traditional control effectors that include ailerons, elevators, and rudder are used. In severe damage situations, these control effectors may not be sufficient to stabilize and maintain good handling qualities of the damaged aircraft. Therefore, any adaptive flight control method must include a control allocation strategy that utilizes other potential control effectors that are otherwise not used in a conventional flight control system. These control effectors can include engine differential thrust for yaw control, wing spoilers for roll control, and wing flap extension or deflection for pitch control. Research in the areas of control redundancy design and reconfigurable control will be conducted to investigate optimal control allocation strategies for these control effectors. The issues of time-scale separation due to actuator dynamics are important for systems with different time latency such as engines and flaps and thus will be an area of adaptive flight control research.[17]

Damage effects can present a serious challenge to conventional flight control systems because the aircraft flight dynamics may deviate from its nominal flight dynamics substantially as result of the degradation in the flight performance of the damaged aircraft. This makes it difficult for the conventional flight control systems to cope with changes in the stability and control of the damaged aircraft. While neural network adaptive control offers a promise of being able to adapt to changes in flight dynamics of damaged aircraft, rigorous validation by simulations and flight testing will be pursued to explore areas of concern in the neural network adaptive flight control. One of the unresolved concerns is the learning characteristics of a neural network. If the dynamic inversion error is large due to a large discrepancy between the true and nominal plant dynamics used in the dynamic inversion control, the learning rate must be set sufficiently high in order for the neural network to reduce the error rapidly. As a consequence of the aggressive learning, the neural network tends to generate high gain control signals that may not be dynamically achievable. This potentially can cause a number of problems including control saturation, load constraints during flight being exceeded, excitation of unmodeled dynamics, and others. One potential solution is to introduce the proposed hybrid adaptive control that incorporates an explicit parameter identification based on an adaptive law derived from the Lyapunov stability method or a recursive least-square method to estimate the true plant dynamics, which would be used for the dynamic inversion control rather than the nominal plant dynamics. This approach potentially offers a way to reduce the dynamic inversion error that the neural network has to compensate for.

Integrated flight dynamics modeling is another area research that addresses interactions among many types of physics problems during flight. An integrated flight dynamics model will be developed to include an aeroservoelasticity interaction model of a flexible-body vehicle dynamics with a propulsion model and its actuator dynamics. This integrated model will capture the combined effects of the 6-dof rigid body dynamics, structural dynamics of airframe, and propulsion model. Post-stall aerodynamics can be included in the aerodynamic coefficients and derivatives which can influence the flutter margin and the aerodynamic damping of the airframe.

Structural interaction with a flight control system is critical to any flight control development.[18–20] Elastic deflection and mode shapes can adversely contribute to the vehicle stability and control, resulting in problems such as flutter, control reversal, structural frequency interaction within the flight control bandwidth, and others. Research in the area of aeroservoelasticity is very important for advancing the knowledge of damage adaptive flight control. Recent advances in fluid-structure interaction modeling using coupled computational fluid dynamics-finite element method provide a predictive capability for aeroservoelastic effects on the stability and control of damaged aircraft.[21] New adaptive flight control methods will need to observe and obey structural load constraints imposed on a damaged airframe. The resulting adaptive flight control methods therefore would be more dynamically achievable. Aeroservoelastic frequency interaction with a safety-critical flight control system will be investigated in order to develop an integrated approach for dealing with potential issues with high frequency signals from elastic modes injecting into the frequency bandwidth of the rigid-body aircraft dynamics. Research in aeroservoelastic filtering and structural identification for flight control will provide methods for assessing the elastic contribution of the airframe and developing adaptive flight control methods that can effectively filter out unwanted structural resonant modes within the flight control bandwidth.

IX. Conclusions

This paper has presented recent results on the modeling, control, and simulation of damaged aircraft as part of the aviation safety research at NASA. The damage effect aerodynamic modeling has been performed to provide an understanding of the control and stability of an asymmetric damaged aircraft. The effects of aerodynamic and control coupling in all the three stability axes are revealed from the modeling results. A 6-dof flight dynamics of asymmetric aircraft is derived in order to account for the effect of the center of gravity shift resulting from the damage. An approach for trimming the damaged aircraft for the translational motion is presented. The trim procedure provides initial estimates of the trim values for the angle of attack, angle of sideslip, and engine thrust. The influence of the control surfaces on these trimmed values is then accounted for by adjusting the initial trim values with the control surface deflections obtained from the flight control. A hybrid direct-indirect neural network adaptive flight control concept has been proposed to provide an opportunity to estimate plant dynamics in conjunction with the current direct adaptive control augmentation strategy. The on-line estimation of the plant dynamics is provided by an adaptive law derived from the Lyapunov stability theory and the recursive least-square method. The adaptive flight control is designed to track a reference model that specifies desired handling characteristics for a class of transport aircraft. The feedback control augmentation uses a proportional and integral scheme to handle errors in the roll, pitch, and yaw rates. A control simulation of the direct adaptive control law is performed in a flight simulator to assess the stability recovery of a damaged generic transport model using the neural network adaptive flight control. The results of the simulation show that the direct neural network control augmentation scheme is able to stabilize a damaged aircraft. In the near future, a control simulation of the hybrid adaptive control law will be conducted to investigate the potential benefits offered by this proposed scheme in reducing the possibility of high gain control in the present direct adaptive control strategy. Moreover, adaptive flight control research will advance the knowledge in the area of integrated flight control with propulsion and airframe effects in order to address interactions between vehicle dynamics, propulsion dynamics, and structural dynamics that may be present. The assumption of rigid-body aircraft flight dynamics no longer holds true as the aircraft will have to be treated as an elastic body. This will give rise to challenges in developing adaptive flight control that can handle aeroservoelastic effects of damaged aircraft.

References

[1] National Transportation Safety Board, C., "In-Flight Separation of Vertical Stabilizer American Airlines Flight 587 Airbus Industrie A300-605R, N14053 Belle Harbor, New York, November 12, 2001", NTSB/AAR-04/04, 2004.

[2] Hughes, D. and Dornheim, M.A., "DHL/EAT Crew Lands A300 With No Hydraulics After Being Hit by Missile", Aviation Week Space & Technology, pp. 42, 12/08/2003.

[3] Kaneshige, J., Bull, J., and Totah, J., "Generic Neural Flight Control and Autopilot System", AIAA Guidance, Navigation, and Control Conference, AIAA-2000-4281, 2000.

[4] Atkins, E., "Dynamic Waypoint Generation Given Reduced Flight Performance", 42nd AIAA Aerospace Sciences Meeting and Exhibit, AIAA-2004-779, 2004.

[5] Jacklin, S.A., Schumann, J.M., Gupta, P.P., Richard, R., Guenther, K., and Soares, F., "Development of Advanced Verification and Validation Procedures and Tools for the Certification of Learning Systems in Aerospace Applications", Proceedings of Infotech@aerospace Conference, Arlington, VA, Sept. 26-29, 2005.

[6] Totah, J., Kinney, D., Kaneshige, J., and Agabon, S., "An Integrated Vehicle Modeling Environment", AIAA Atmospheric Flight Mechanics Conference and Exhibit, AIAA-1999-4106, 1999.

[7] Steinberg, M.L., "A Comparison of Intelligent, Adaptive, and Nonlinear Flight Control Laws", AIAA Guidance, Navigation, and Control Conference, AIAA-1999-4044, 1999.

[8] Rohrs, C.E., Valavani, L., Athans, M., and Stein, G., "Robustness of Continuous-Time Adaptive Control Algorithms in the Presence of Unmodeled Dynamics", IEEE Transactions on Automatic Control, Vol AC-30, No. 9, pp. 881-889, 1985.

[9] Ioannu, P.A. and Sun, J. *Robust Adaptive Control*, Prentice-Hall, 1996.

[10] Eberhart, R.L. and Ward, D.G., "Indirect Adaptive Flight Control System Interactions", International Journal of Robust and Nonlinear Control, Vol. 9, pp. 1013-1031, 1999.

[11] Rysdyk, R.T. and Calise, A.J., "Fault Tolerant Flight Control via Adaptive Neural Network Augmentation", AIAA Guidance, Navigation, and Control Conference, AIAA-1998-4483, 1998.

[12] Kim, B.S. and Calise, A.J., "Nonlinear Flight Control Using Neural Networks", Journal of Guidance, Control, and Dynamics, Vol. 20, No. 1, pp. 26-33, 1997.

[13] Johnson, E.N., Calise, A.J., El-Shirbiny, H.A., and Rysdyk, R.T., "Feeback Linearization with Neural Network Augmentation Applied to X-33 Attitude Control", AIAA Guidance, Navigation, and Control Conference, AIAA-2000-4157, 2000.

[14] Narendra, K.S. and Annaswamy, A.M., "A New Adaptive Law for Robust Adaptation Without Persistent Excitation", IEEE Transactions on Automatic Control, Vol. AC-32, No. 2, pp. 134-145, 1987.

[15] Lewis, F.W., Jagannathan, S., and Yesildirak, A., *Neural Network Control of Robot Manipulators and Non-Linear Systems*, CRC, 1998

[16] Krishnakumar, K., Limes, G., Gundy-Burlet, K., and Bryant, D., "An Adaptive Critic Approach to Reference Model Adaptation", AIAA Guidance, Navigation, and Control Conference, AIAA-2003-5790, 2003.

[17] Naidu, D.S. and Calise, A.J., "Singular Perturbations and Time Scales in Guidance and Control of Aerospace Systems: A Survey", Journal of Guidance, Control, and Dynamics, Vol. 24, No. 6, 0731-5090, pp. 1057-1078, 2001.

[18] Brenner, M.J. and Prazenica, R.J., "Aeroservoelastic Model Validation and Test Data Analysis of the F/A-18 Active Aeroelastic Wing", NASA/TM-2003-212021, 2003.

[19] Meirovitch, L. and Tuzcu, I, "Integrated Approach to Flight Dynamics and Aeroservoelasticity of Whole Flexible Aircraft - Part I: System Modeling", AIAA Guidance, Navigation, and Control Conference, AIAA-2002-4747, 2002.

[20] Meirovitch, L. and Tuzcu, I, "Integrated Approach to Flight Dynamics and Aeroservoelasticity of Whole Flexible Aircraft - Part II: Control Design", AIAA Guidance, Navigation, and Control Conference, AIAA-2002-5055, 2002.

[21] Livne, E., "Future of Airplane Aeroelasticity", Journal of Aircraft, Vol. 40, No. 6, 2003.